# THE EFFECT OF CATALYSTS ON COAL GASIFICATION

Reuel Shinnar
C.A. Feng
Alan I. Avidan

Department of Chemical Engineering
The City College of the
City University of New York
New York, New York 10031

## INTRODUCTION

There have been a number of studies dealing with the impact of various catalysts in coal gasification (1,2,3,4,5) and one catalytic process for SNG (6) has been operated successfully in a large pilot plant. This paper analyzes the potential value of catalysts in coal gasification. The paper will first discuss what is the proper operating range for a gasifier by reviewing the thermodynamic and kinetic constraints of coal gasifiers, then analyze the question as to what type of catalyst is really required. Both syngas processes and SNG production will be discussed.

There are a few separate areas in which catalysts would be valuable in coal gasification.

1) SNG Production. In SNG production it has already been shown (8) that there would be a significant process advantage for a catalyst that could operate at 1000-1100°F. The global equilibrium at these temperatures contains mainly $CH_4$ and $CO_2$. The reaction heat requirements are low and can be supplied by superheated steam, which simplifies the process considerably. Steam conversion is low, but this disadvantage is overcome by the other advantages of such a simple process. The lowest operating temperature that has been achieved with good conversion of carbon and steam is 1300°F. Operating at 1300° requires a very high concentration of potassium hydroxide or potassium carbonate in the coal. As recovery is difficult, the high concentration of potassium increases catalyst losses and reduces the economic incentive. At a temperature of 1300°F significant amounts of CO and $H_2$ are formed. The process developed by Exxon separates these gases from the methane and recycles them to the reactor. This requires a catalyst with a high methanation activity. We will show that a catalyst operating at 1400-1500° could also be acceptable but the process would have to be modified. By proper modification this process should be competitive with the process proposed by Exxon and could utilize cheaper catalysts, or lower catalyst concentrations.

2) Syngas Generation. In syngas generation the thermodynamic optimum (8) is at conditions where coal gasification is fast. However, for many coals it is difficult to operate at these conditions. The only gasifier that has achieved operation close to the thermodynamic optimum is the British Gas Corporation slagging-type gasifier or BGC slagger. However, the BGC slagger is not suitable for all coals. In fluid bed gasifiers, one has to operate at lower temperatures to prevent agglomeration or ash melting. Under such conditions high conversion of the char is difficult as the gasification reaction is very slow at temperatures below 1700°F if char conversion is to exceed 70% (9).

The Winkler gasifier as well as present second generation fluid bed gasifiers for syngas all operate in a partial oxidation regime which reduces their thermal efficiency and increases the amount of oxygen required. A proper catalyst operating at 1500-1600°F could allow high

carbon and steam conversion and could potentially solve the inherent operating problems faced by all fluid bed gasifiers.

3) Gas Cleanup. The third area in which catalysts could significantly contribute to improved coal gasification processes is in the area of gas cleanup. There is a strong advantage in devolatilizing the coal prior to feeding it to the gasifier. However, this leads to the formation of tars and phenols which require expensive gas cleanup, and prevent efficient heat recovery from the product gas. If those products could be cracked at high temperatures, preferably in the devolatilization zone itself to methane and char, this would simplify the process scheme.

4) Improved Devolatilization. In a two-stage process, the results obtained in the devolatilization zone are very important. The amount of coal devolatilized in this stage as well as the product distribution strongly depends on the devolatilization conditions. A proper catalyst could change both the product yield and product distribution in the devolatilizaton zone.

Aside from the development of the Exxon process, most work on the effect of catalysts has concentrated on item two: acceleration of the gasification reaction. Almost no measurements are available as to whether these catalysts also accelerate the methane formation reaction, nor is there any reported study of the effect of catalysts on items 3 and 4 listed above.

Let us now shortly discuss each item separately.

1) Use of Catalysts in SNG Production

The thermodynamic and kinetic constraints of SNG processes are discussed in detail in (ref. 10), and we will here only summarize them.

Present catalysts do not promote the direct reactions

$$C + H_2O \rightarrow 1/2CH_4 + 1/2CO_2 \qquad 1)$$

$$1.5C + H_2O \rightarrow 1/2CH_4 + CO \qquad 2)$$

In present gasifiers and catalysts, methane is formed in several ways:

1) devolatilization of coal
2) reaction between CO and $H_2O$ or CO and $H_2$
3) hydrogasification of coal

The CO, $H_2$ and $CO_2$ are formed by the reaction

$$C + H_2O \rightarrow CO + H_2 \qquad 3)$$

$$CO + H_2O \rightarrow CO_2 + H_2 \qquad 4)$$

Methanation of CO (or $CO_2$) with hydrogen by the reaction

$$CO + 3H_2 \rightarrow CH_4 + H_2O \qquad 5)$$

requires (10) that the $CH_4$ concentration is lower than:

$$[CH_4] < \frac{[H_2]^3[CO]}{[H_2O]} K_P \qquad 6)$$

where $K_p$ is the equilibrium constant of reaction 5.
This only occurs when the $CH_4$ concentration is less than required by global equilibrium.

In the gasification zone the maximum amount of methane that can be generated by gasification is therefore limited by global equilibrium over char (10). There is one exception. At high temperatures the amount of methane generated by devolatilization is larger than is consistent with global equilibrium. This excess methane will react

with steam in the reverse reaction (10). However, if this reaction is slow, the methane concentration at the gasifier outlet will be above the global equilibrium.

If SNG is the desired product, then there is an advantage to increasing the direct methane yield in the gasifier. We define here direct methane yield for an SNG process as

$$\text{Direct methane yield} = \frac{CH_4}{CH_4 + \frac{1}{4}(CO + H_2)}$$

where $[CH_4]$, $[CO]$ and $[H_2]$ are the molar fractions of these compounds in the gasifier outlet. Increasing this ratio has two advantages for SNG production.

1) It reduces the cleanup cost of the product gas.
2) It reduces the heat requirements in the gasification zone (or the recycle requirements in the Exxon process). This is only correct if the methane formation occurs in the gasification zone. If the CO formed in a high temperature zone reacts to methane in a low temperature zone, this does not reduce the heat requirements.

The direct yield can be increased by proper utilization of the methane formed in the devolatilization zone (10). This requires a countercurrent scheme such as the one given in Fig. 1, model 2. This scheme can be approximated in a fluid bed by using a two-stage gasifier such as in model 3. Both countercurrent schemes have the further advantage that the coal is preheated with gasifier effluents. The difference in the thermodynamic constraints between model 2 and 3 is small. We will therefore use model 3 for presenting our results.

The maximum direct methane yield will, therefore, depend also on gasifier design. In a countercurrent or moving bed or two-stage gasifier, the methane from devolatilization has no impact on the global equilibrium. In a one-stage gasifier this methane is generated in the gasification zone and affects the equilibrium.

There are no accurate estimates as to how much methane is formed by devolatilization. This strongly depends on coal, operating conditions, temperature and of partial pressure of steam and hydrogen The best estimates we have are from the BGC slagger and the Dry Ash Lurgi, though in both cases the flow is countercurrent and part of the methane could be formed by methanation in the cool zone just below the devolatilization zone.

Our estimates of the methane formed by devolatilization are taken from ref. 11. There is one more factor that affects direct methane yield. Without a catalyst methanation is slow. Some catalysts promote gasification (reaction 3), but do not promote methanation. We can therefore look at a limiting case in which no methanation occurs in the gasifier.

In Fig. 2 the direct methane yield ratio is plotted for several types of gasifiers operating at global equilibrium with Eastern coal. We choose Eastern coal as our main example since the main need for a catalyst is in the gasification of Eastern caking coals. We give direct methane yield ratio for two pressures (400 and 1000 psia) and for two gasifier models. One, (curve B), is a single stage mixed gasifier. For it we present two limiting cases. In the first we assume global equilibrium in the gasification zone. In the second (curve D) we assume that no methanation occurs in the gasifier, only devolatilization. If the methane yield at global equilibrium is higher than that formed by devolatilization, we assume it to be equal to that formed by devolatilization. If it is lower, we assume that it is equal to global equilibrium. This assumption makes sense at high temperature

since the methane steam reaction is fast without a catalyst.

We also give the results for a two-stage countercurrent gasifier (model III). Here, we also give two cases. One (curve A) in which the methane formation in the gasification zone is at global equilibrium. The other (curve C) where no methane formation occurs in the gasification zone.

Fig. 2 is based on an oxygen steam gasifier operating at equilibrium. Oxygen and steam are fed to the gasifier at 1000°F. We note that at low temperatures (below 1700°F) there is very little difference between curve C and D. At still lower temperatures the difference between A and B disappears. The main advantage of prior devolatilization is at higher temperatures. At 1500°F the advantage in terms of direct methane yield is significant only for the case where we have a catalyst that promotes methanation in the gasification zone.

We note in Fig. 2 that while increased pressure (Fig. 2b) increases the direct methane yield, the trends are similar in both cases. The main impact of increased pressure is to shift the curves towards higher temperatures.

In Fig. 3 we give the oxygen and steam requirements for SNG production as a function of temperature for a two-stage countercurrent and a one-mixed-stage gasifier. The oxygen and steam requirement are given in the form of the performance parameter proposed in ref. (7) and (8).

$$E_{CH_4} = \frac{H_2O + 4O_2}{CO + H_2 + 4CH_4}$$

which is proportional to the energy requirements to generate the feed for 0.25 mole $CH_4$. (The 0.25 $CH_4$ was chosen to make the parameter comparable to the performance parameter used for syngas and fuel gas, see later).

This parameter is an approximate performance parameter which gives different weight to the oxygen and steam requirements in the feed. This weighting factor is based on energy requirement of the feed and correlates quite well with total cost of the feed preparation. Oxygen use also involves another penalty. If its use is more than required by the stoichiometry (8,13), it reduces the cold gas efficiency. To evaluate this we need a complete heat balance of the gasifier. However, simplified performance criteria such as given here, give a reasonable picture of the impact of process parameters on cost and thermal efficiency.

In Fig. 3 we also give actual results for different gasifiers for Eastern coal. None of these is really commercial, but the data in either for a semi-commercial operation (Dry Ash Lurgi, BGC slagger, Texaco), or a large pilot plant (Shell, Westinghouse). We also give the performance of the Exxon process in an equivalent form. The Exxon gasifier does not use oxygen. It reduces the heat of reaction required by cryogenically separating the CO and $H_2$ from the methane and recycling them to the gasifier. The remaining small heat of reaction is supplied by superheating the recycle stream to 1500°F by burning part of the product gas. We try to present this gasifier here in an equivalent form by using an equivalent amount of oxygen. This is obtained by computing the energy used by the cryogenic separation process per mole net methane produced and converting it to oxygen by computing the number of moles of oxygen that could be produced by the same energy. This is reasonable as the cost of an oxygen plant and of the cryogenic separator are quite similar if based on the same energy consumption.

We note that a process operating with oxygen at 1500°F close to

equilibrium would have an advantage in terms of energy expanded over the Exxon process as proposed.

Figs. 2, 3 and 4 give us a good picture of the potential value of a catalyst that operates at low temperatures. At high temperatures such as in a slagger, it would not affect steam and oxygen consumption. But at low temperatures such as 1400°-1500°F its effect would be very beneficial. However, in this case it is essential that the catalyst promotes the methanation reaction.

A two-stage scheme based on such a catalyst at 1500°F would be competitive in terms of efficiency with the Exxon gasifier operating at 1300°F. Its overall thermal efficiency would be slightly better or equal and investment cost would be lower especially if the higher temperature leads to faster reactions and lower residence times.

At 1400°-1500°F there is very little chance of ash agglomeration. The main problem would be the agglomeration of caking coals. Pretreatment with a catalyst seems to prevent this phenomenon. Another way out is use of a high velocity mixing zone into which the fresh coal is introduced.

Introduction of fresh oxygen can also cause a locally excessive temperature that would lead to agglomeration. One way of minimizing this is to introduce the oxygen together with the steam and some recycle gas (or coal fines). This would raise steam temperature in the feed. By proper design of the steam nozzles and the mixing zone, this heat would be easier to dissipate than the heat generated by direct combr?r?r?rustion of oxygen inside the gasifier.

?r There is therefore a strong incentive to look for cheap catalysts?r operating at 1400°F to 1500°F provided they not only acceler?r?r?rate the gasification reaction but also the methanation reaction. If they promote gasification only, we really deal with a case identical to fuel or syngas production which will be discussed in the next section.

One might even consider using a combination of two catalysts as it is not clear that a cheap efficient gasification catalyst operating at 1500°F will also promote methanation. Iron is a good methanation catalyst but loses its activity in the presence of sulphur. Sulphur resistant methanation catalysts are known but are expensive.

Regrettably, most studies in catalysis in coal gasification only report the gasification rate and do not measure the effect of the catalyst on methanation.

If such a catalyst would operate at 1100-1200°F, then one would be able to get a very simple process of supplying the process heat with superheated steam in a one-stage fluid bed. At 1400-1500°F the most promising candidate would be a two-stage fluid bed, the upper stage operating around 1200°F and the lower stage at 1400-1500°F. Heat could be supplied either by direct oxygen introduction or by superheating the steam to high temperatures with oxygen and raw product gas.

2) Syngas and Fuel Production

Syngas production is similar to fuel gas production, with one important difference. In fuel gas production the percentage of methane in the gas is irrelevant. In syngas production there is a premium for methane free syngas.

For some syngas processes such as methanol and Fischer Tropsch, the presence of methane up to a certain amount (10% of syngas) has only a low penalty in the syngas conversion process. On the other hand, there is a severe penalty to operate a gasifier such that the methane formed by devolatilization is destroyed. The difference in cost for syngas from a BGC slagger as compared to a Shell or Texaco gasifier is such that the incremental methane formed in the slagger is very cheap, both in terms of incremental investment and coal use.

We therefore would like to have a gasifier such as the slagger.

Fig. 5 compares the oxygen and steam requirements (reported as $H_2O + 4O_2$) for a unit of syngas. It is just a replot of Fig. 3 as we deal here with the same constraints. We give here methane a reduced value (half of final product), and therefore use as a criterion

$$E_S = \frac{H_2O + 4O_2}{CO + H_2 + 2CH_4}$$

For fuel gas the denominator would change to $CO+0.85H_2+2.83CH_4$ (see ref. 8). But here we are interested in syngas. The overall conclusions for fuel gas would be very similar.

Looking at this ratio for the various cases in Fig. 5, we note again the advantage of a two-stage countercurrent unit. We also note that the optimum is clearly at a high temperature especially if we want to minimize methane at the same thermal efficiency. A catalyst would not change that. All a catalyst would do is to allow operation at lower temperature close to the equilibrium line.

That means we would have to pay a price for operating at lower temperature. This is justified if we need a gasifier for coals not suited for the slagger, or want to handle fines. It may also lead to simpler, more robust gasifiers.

Another goal would be a gasifier for a smaller plant in which simplicity has a high value. The tars found in the slagger make the total system quite complex and less suitable for smaller sized plants.

Here a gasifier operating close to equilibrium at temperatures around 1500-1800°F could have significant advantages. We want the temperature to be as high as possible, close to the limit dictated by agglomeration. However, gasification at these temperatures is slow. This is especially true at high carbon conversion. Gasification rate seems to drop severely as conversion exceeds 70% (9). One way to achieve high conversion is to operate with excess oxygen. Partial combustion of char to CO is fast. One then has to remove the excess heat. One can either operate at very high temperatures in a single stage gasifier (Shell, Koppers Totzek and Texaco) or use excess steam or recycle gas as a coolant (Winkler, Westinghouse). This reduces the thermal efficiency, as can be noted from Figs. 4 and 5.

All present fluid bed gasifiers operate in the partial combustion regime, using large excesses of oxygen and steam as compared to equilibrium requirement. We define this regime of the oxygen-to-converted coal ratio (8). If this exceeds the ratio required to convert all carbon to CO we call the gasifier a partial combustor.

Ref. (8) shows that the critical ratio of $O_2$ to carbon that distinguishes gasification from partial combustion can be defined for a coal of composition $CH_aO_b$ as

$$R_{crit} = \frac{1 - b}{2}$$

The values of R for an equilibrium gasifier without methane formation in the gasification zone was given in Fig. 4. Values of the Westinghouse pilot plant, as well as other gasifiers, are given in the same plot. We note that while all equilibrium gasifiers have a value of R less than $R_{critical}$ only the countercurrent gasifiers achieve such low value and in that sense they are at present the only true gasifiers. Cheap catalysts could allow fluid beds to operate in the same regime and thereby increase their efficiency.

Here, the only catalyst property that counts is promotion of reaction (3) at high coal conversion and temperatures of about 1600°F. Several cheap catalysts tested seem to have the property and merit further investigation.

3) Devolatilization

One potential area of catalysis that has been completely neglected is the direct reaction of coal with $H_2$ and steam. When coal devolatilizes primary pyrolysis products are formed (1,12,13,14), which then either decompose into char and gases or react with steam or hydrogen. Sometimes this is called active char, but we really deal with a reaction of pyrolysis intermediates with steam (or hydrogen). This reaction can be promoted by high temperatures and high steam or hydrogen pressure. This involves other penalties. An attractive alternative would be a cheap catalyst that promotes the reaction of pyrolysis products with steam. To be really attractive this catalyst should preferably also promote the decomposition of tars and phenols and should operate at moderate pressures (400 psi) and low temperatures (less than 1400°F).

Shinnar et al. (10) discuss thermodynamic reasons why direct reaction of coal with steam is not likely. It is much more likely to involve an irreversible intermediate step, which would lead to the overall reaction

coal + steam (or hydrogen) -> products + char

The amount of char could be quite small (less than 40%). Study of such reaction in the presence of catalysts at reasonable temperatures and pressures could be of significant value. Another item is the decomposition of tars and phenols found directly in the devolatilization stage, at reasonably low temperatures (1100-1200°F). Here there are a range of catalysts that could have this effect. The problem is that such catalysts must be effective in reasonably small amounts. Otherwise, the ash removal problem becomes more difficult.

4) Gas cleanup

Devolatilization of coal leads, in addition, to methane, CO and $H_2$, also to tars and phenols. In a two-stage fluid bed it would be desirable to decompose them in the devolatilization zone, which should be possible and could be one of the main advantages of fluid bed gasifiers. However, in a slagger this is impossible and it would be very desirable if we had a catalyst which could decompose these tars and oxygenate with low excess of steam, which is probably very hard to achieve. However, the gas in a Dry Ash Lurgi used for Western coals contains almost 50% excess steam. A catalyst that decomposes all phenols and tars would make gas cleanup and waste water removal simpler and cheaper for such a gasifier and could have significant value if Dry Ash Lurgi gasifiers ever become more widely used.

Summary and Conclusion

Several key areas have been identified in which proper, cheap disposable catalysts could have significant impact on coal gasification processes.

For SNG production it would be desirable to find a cheaper throwaway catalyst operating at low temperatures, preferably below 1200°F. As such a catalyst is not in sight, one could also achieve significant advantages with a catalyst operating at 1400-1500°F provided the catalyst (or mixture of catalysts) promotes both gasification and methanation of CO. A gasifier design that could utilize such a catalyst in an optimal way is described.

A catalyst that would promote direct formation of methane (without CO and $H_2$ as intermediate) would be desirable at high temperatures but no such catalyst is in sight.

For syngas production the advantages are smaller and we require a catalyst that promotes gasification without promoting methanation. Such a catalyst could overcome the inherent disadvantages of fluid beds and allow development of efficient fluid bed gasifiers.

Another area discussed is catalysts that would promote better yields in the devolatilization section by promoting the reactions of

pyrolysis products with steam at low temperatures and pressures, to prevent their polymerization.

Also of potential importance is the catalytic decomposition of tars and oxygenated compounds in the offgases of a Lurgi Dry Ash gasifier.

References


1) Walker, P.L. et al. Kinetics of Coal Pyrolysis and Gasification, DOE Report DE-83012279 (1983).
2) Cabrera, A.L., Heinemann, H., Somooryai, G.A. "Methane Production from Catalyzed Reaction of Graphite and Water Vapor at Low Temperatures (500-600 K)", LBL-12812, 1981.
3) McKee, D.W. "The Catalyzed Gasification Reactions of Carbon," Chemistry and Physics of Carbon, (Ed. P.L. Walker, Jr. and P.A. Thrower), Marcel Dekker Inc., New York), 16, 1(1981).
4) McCoy, L.R. et al., "Investigation of Coal Gasification Catalysis Reaction Mechanism," Quarterly Report, Sept. 1981, Rockwell Science Center, DOE Contract DE-AC21-80MC14592.
5) Kosky, P.G. et al. Coal Gasification Catalysis Mechanism, DOE Report DE-82013824 (1982).
6) Exxon Research & Engineering Co. "Exxon Catalytic Coal Gasification Process", FE-2369-24, 1978.
7) Shinnar, R., Kuo, J.C.W. "Gasifier Study for Mobil Coal to Gasoline Processes", FE-2766-13, 1978.
8) Shinnar, R. Thermodynamic and Process Constraints in Coal Gasification and their Economic Impact. Paper given at METC Symposium on Coal Gasification, Morgantown, November 1983.
9) Johnson, J.L. Adv. Chem. Ser. 1974, No. 131, 145.
10) Shinnar, R., Fortuna, G. and Shapira, D. IEC Process Design and Development 21, 728(1982).
11) Yoon, H., Wei, J., Denn, M.M. "Modelling and Analysis of Moving Bed Coal Gasifiers", Final Report, EPRI AF-590, 1977.
12) Zaharadnik, R.L., Grace, R.J. Adv. Chem. Ser. 1974, No. 131, 127.
13) Gavalas, G.R. Coal Pyrolysis, Elsevier, New York 1982.
14) Solomon, P.R. and Colbet, M.B., 17th International Symposium on Combustion, The Combustion Institute, Pittsburgh 1979.

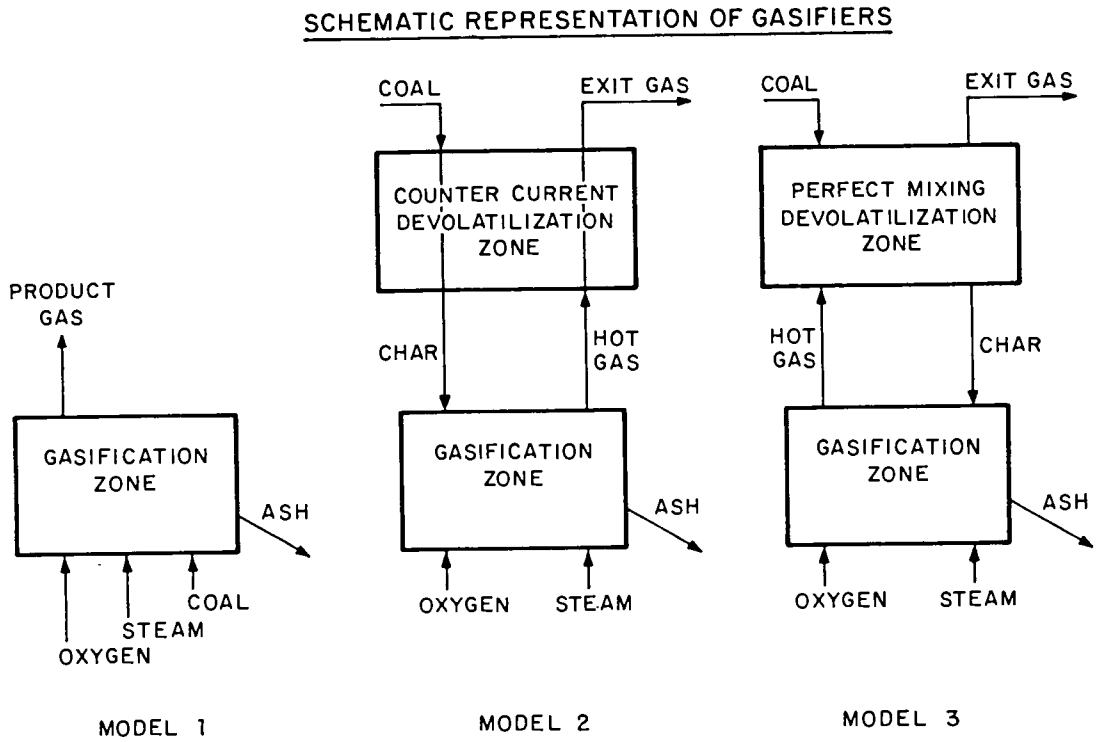


Fig. 1. Schematic Representation of Gasifier Models.

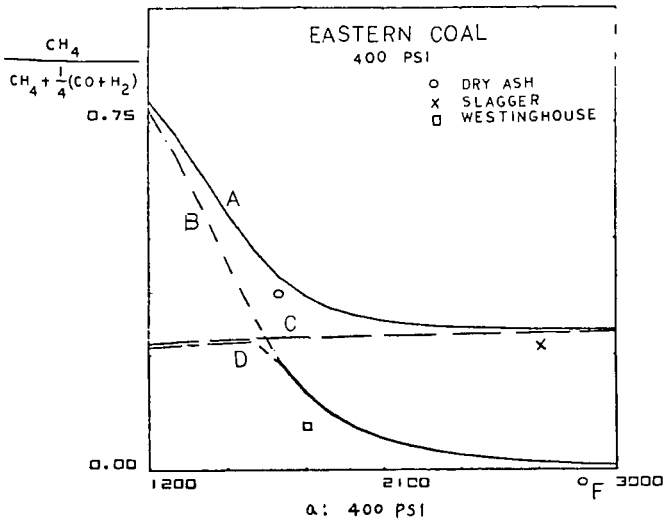


a: 400 PSI

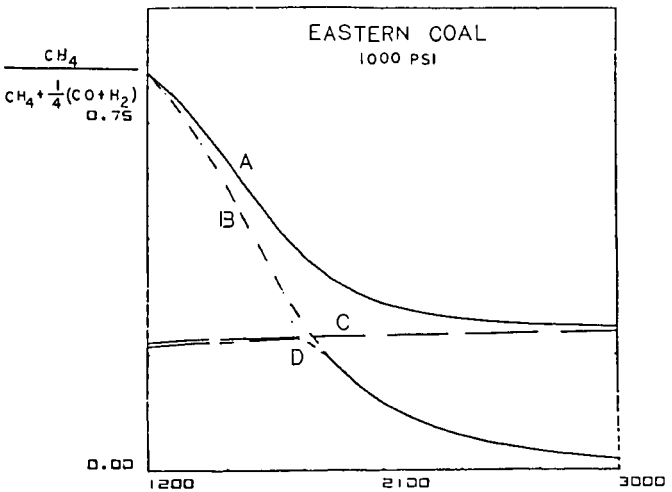


b: 1000 PSI

Fig. 2. Direct Methane Yield in a Steam Oxygen-Blown Coal Gasifier at Global Equilibrium. Effect of pressure, temperature, gasifier design and promotion of the methanation reaction.

A) Two-stage countercurrent gasifier (model III, Fig. 1): Devolatilization in low temperature stage (1000°F). Global equilibrium over char in high temperature stage. (Temperature shown is temperature of high temperature stage).
B) One-stage mixed gasifier, global equilibrium.
C) Similar to A, but no methane formation in gasifier stage.
D) One-stage mixed gasifier, with devolatilization (see text).

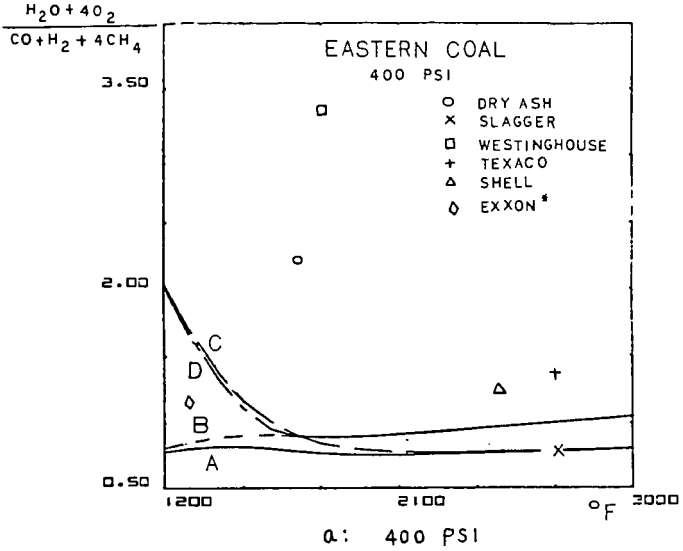


a: 400 PSI

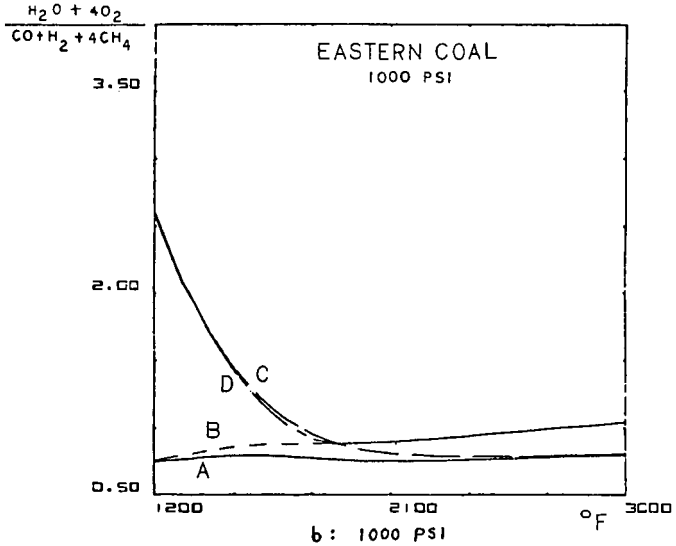


b: 1000 PSI

Fig. 3. Oxygen and steam requirements for gasifiers in Figure 1. For explanation of curves see Figure 2.
*For Exxon gasifier see text for explanation.

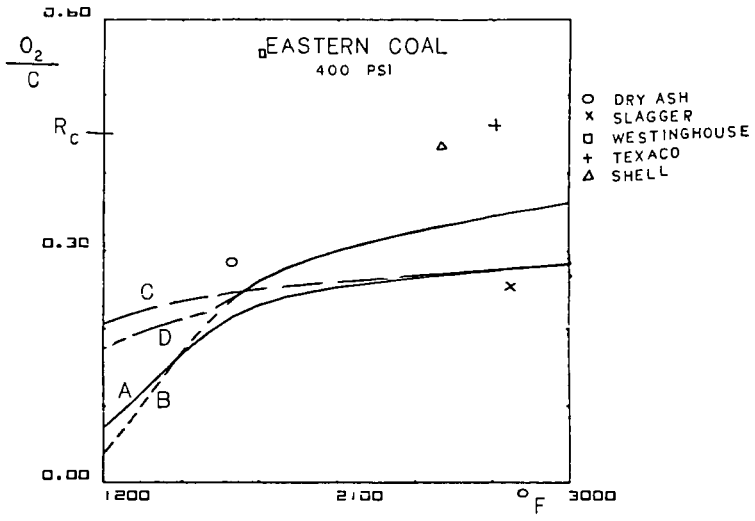


a: 400 PSI

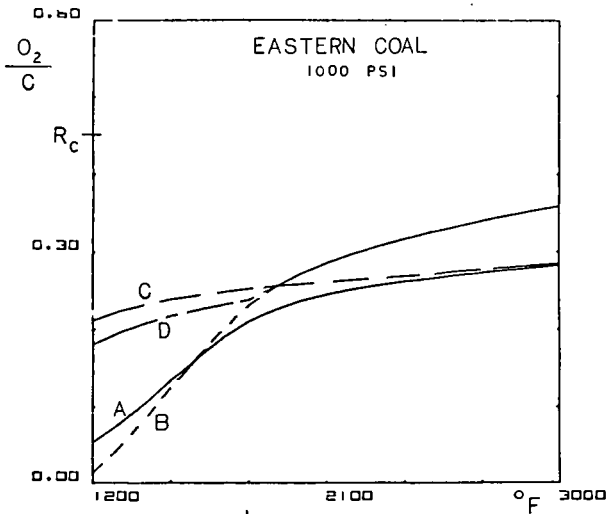


b: 1000 PSI

Fig. 4. Oxygen to carbon ratio for gasifiers in Figure 3.

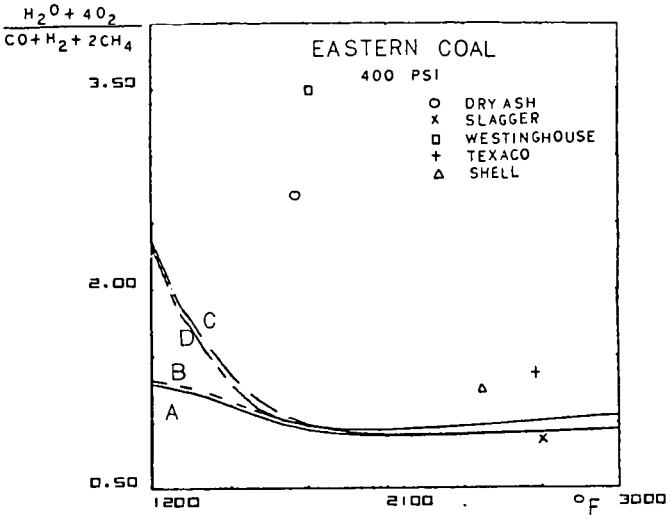


a: 400 PSI

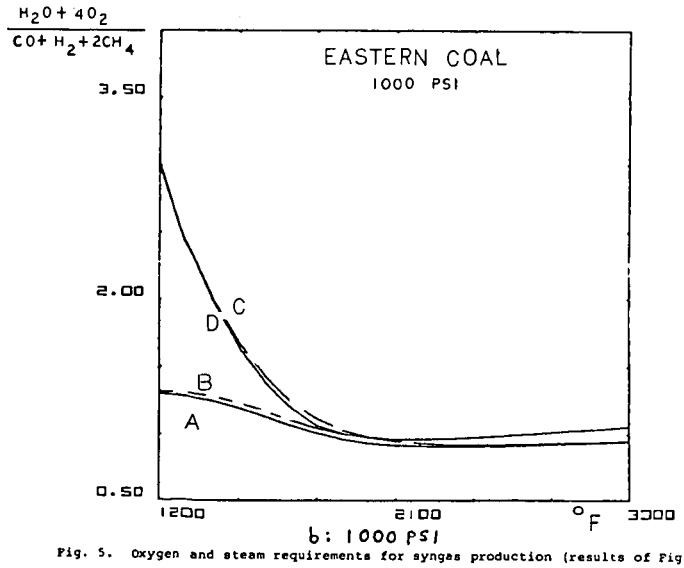


b: 1000 PSI

Fig. 5. Oxygen and steam requirements for syngas production (results of Fig. 3 replotted).

# DETERMINATION OF THE INTRINSIC ACTIVITY AND EFFECTIVE DIFFUSIVITY OF AGED COAL LIQUEFACTION CATALYSTS*

H. P. Stephens and F. V. Stohl

Sandia National Laboratories, Albuquerque, NM 87185

## INTRODUCTION

Although severe, rapid catalyst deactivation remains a major economic impediment to the production of liquid fuels from coal by direct processing, there have been few quantitative investigations of aged catalyst intrinsic activity and effective diffusivity. This study reports a method for determining these important properties under experimental conditions that accurately model actual conditions for the processing of coal-derived liquids. The power of the technique has been demonstrated by determination of the intrinsic hydrogenation activity and effective diffusivity of catalysts obtained from the Wilsonville, Alabama coal liquefaction test facility. In addition, modeling of the experimental results has conclusively identified the modes of catalyst deactivation.

The values of intrinsic catalyst activity and effective diffusivity reported here are based on kinetic measurements of the catalytic hydrogenation of pyrene. Pyrene was chosen as a chemical probe of these properties because it appears to play a key role (1,2) as a hydrogen transfer agent in coal liquefaction: hydropyrenes are good hydrogen donors; they have low vapor pressures at liquefaction temperatures; and significant amounts are found in liquefaction solvents (3).

From determination of the pyrene hydrogenation rate constants for pairs of experiments, one with powdered catalyst and the other with whole extrudates, the fraction deactivated and the Thiele modulus, which relates the intrinsic rate constant to the extrudate effective diffusivity, were determined. Experiments with fresh, aged and regenerated catalysts have allowed the contribution of deactivation due to metallic contaminants to be separated from that due to carbonaceous material, and thus has allowed the mode of deactivation for each contaminant to be determined.

## THEORY OF DIFFUSION AND REACTION OF PYRENE IN CATALYSTS

### Pyrene Hydrogenation Kinetics

Although pyrene (Py) is catalytically hydrogenated to several products, under the conditions used in this study the major product is 4,5-dihydropyrene ($H_2Py$). Previous work (4,5) has shown that the hydrogenation of pyrene (reaction [1]) can be precisely described by pseudo first order reversible kinetics (equation [2]):

$$H_2(g) + Py \underset{k_{-1}}{\overset{k_1}{\rightleftharpoons}} H_2Py \qquad [1]$$

* This work supported by the U. S. Dept. of Energy at Sandia National Laboratories under contract DE-AC04-76DP00789.

$$\ln \frac{X_e}{X_e - X_t} = kt \qquad [2]$$

where k is the sum of the forward ($k_1$) and reverse ($k_{-1}$) rate constants, and $X_t$ and $X_e$ are the extents of reaction of pyrene to dihydropyrene at time t and equilibrium. $X_t$ is calculated directly from the experimental product distribution:

$$X_t = \frac{[H_2Py]_t}{[Py]_t + [H_2Py]_t} \qquad [3]$$

$X_e$ is calculated from the experimentally observed hydrogen pressure p and the pressure equilibrium constant $K_p$:

$$X_e = \frac{[H_2Py]_e}{[Py]_e + [H_2Py]_e} = \frac{pK_p}{1 + pK_p} \qquad [4]$$

where:

$$K_p = \frac{1}{p} \frac{[H_2Py]_e}{[Py]_e} \qquad [5]$$

Catalyst Activity and Effective Diffusivity

Fresh Catalysts. For fresh catalyst extrudates, the fraction of the surface area used for chemical reaction is given by the effectiveness factor ε, defined as the ratio of the actual reaction rate for the extrudate to the intrinsic reaction rate (i.e., without diffusion resistance). The effectiveness factor may be determined from the intrinsic rate constant ($k_i$) for experiments with finely powdered catalyst and the apparent rate constant ($k_a$) for experiments with whole catalyst extrudates

$$\varepsilon = \frac{k_a}{k_i} \qquad [6]$$

Upon solving the differential equation for simultaneous diffusion and reaction in a catalyst particle (6), it is found that the effectiveness factor is a function of the Thiele modulus, h:

$$\varepsilon = \frac{\tanh (h)}{h} \qquad [7]$$

The Thiele modulus for catalyst pellets of all shapes may be closely approximated (7) by the following equation:

$$h = \frac{V_p}{S_x} \sqrt{\frac{\rho k_w}{D_e}} \qquad [8]$$

where $V_p$ and $S_x$ are the volume and external surface area of the catalyst pellet, $\rho$ is the pellet density, $k_w$ is the intrinsic rate constant on a catalyst weight (w) basis [equal to $(k_1 + k_{-1})/w$ for reversible reactions (6)] and De is the effective diffusivity (diffusion coefficient within the catalyst pellet). Because the Thiele modulus can be determined from equation [7] using the effectiveness factor given by equation [6], the effective diffusivity can be readily calculated by rearrangement of equation [8]:

$$D_e = \left(\frac{V_p}{S_x}\right)^2 \left(\frac{1}{h}\right)^2 \rho k_w \qquad [9]$$

Aged and Regenerated Catalysts. The relationship of the fraction F of aged pellet activity remaining to the Thiele modulus h and fraction poisoned $\alpha$ is given by the following equations for the limiting cases of uniform and pore mouth poisoning (8):

Uniform poisoning -

$$F = \left[\frac{\tanh\left(h\sqrt{1-\alpha}\right)}{\tanh(h)}\right]\sqrt{1-\alpha} \qquad [10]$$

Pore mouth poisoning -

$$F = \left[\frac{\tanh[(1-\alpha)h]}{\tanh(h)}\right]\left[\frac{1}{1+\alpha h \tanh[(1-\alpha)h]}\right] \qquad [11]$$

These equations were derived assuming deactivation results only from poisoning. However, coal liquefaction catalysts may deactivate as a result of the combined effects of uniform and pore mouth poisoning, and pore size reduction. We therefore modified equation [11] to include all of these modes of deactivation. The resulting equation models the fraction of pellet activity remaining for an aged catalyst which may have a completely deactivated shell due to pore mouth poisoning, a partially deactivated core due to uniform poisoning and an effective diffusivity which is less than that of the fresh catalyst:

$$F = \left[\frac{\tanh[(1-\alpha_s)h]}{\tanh(h_f)}\right]\left[\frac{1}{1+\alpha_s h \tanh[(1-\alpha_s)h]}\right]\sqrt{\frac{\rho k_c D_e}{\rho_f k_f D_{ef}}} \qquad [12]$$

where $h_f$, $\rho_f$, $k_f$ and $D_{ef}$ are the Thiele modulus, pellet density, rate constant and effective diffusivity for the fresh catalyst; h, $\rho$ and $D_e$ are the corresponding parameters for the aged catalyst; $\alpha_s$ is the fraction deactivated by shell progressive pore mouth poisoning; and $k_c$ is the rate constant of the partially deactivated catalyst core given by:

$$k_c = (1 - \alpha_c)\, k_f \qquad [13]$$

where $\alpha_c$ is the fraction of the core that is deactivated. Use of equation [12] to calculate effective diffusivities for aged and regenerated catalysts is discussed in the Results Section.

## EXPERIMENTAL

### Catalysts

Extrudates (0.8 mm diameter by 4 mm long) of Shell 324M, a 12.4% Mo, 2.8% Ni on alumina catalyst used in second-stage processing (9) of liquids derived from Illinois No. 6 (Burning Star) coal were obtained from the Wilsonville, Alabama coal liquefaction test facility. Fresh catalyst samples, used for baseline activity comparisons, were activated by presulfiding for 6 hours at 400°C and atmospheric pressure using a mixture of 10 mole % $H_2S$ in $H_2$. Aged catalysts consisted of samples periodically withdrawn from the hydroprocessing reactor during run 242. In addition, samples were obtained from runs 242, 243 and 244, following process catalyst presulfiding with dimethyldisulfide in an oil vehicle, but prior to coal-derived liquid processing. Upon receipt, the aged catalysts, which were shipped in toluene, were Soxhlet extracted with tetrahydrofuran (THF) to remove as much of the soluble hydrocarbons as possible, then dried under vacuum at 100°C to remove traces of THF.

To investigate the effect of deactivation by contaminant metals, carbonaceous material was removed from the aged catalysts by slowly heating the extrudates to 500°C in air over a period of several hours and leaving them at this temperature overnight. These regenerated samples were then resulfided by the same method used for presulfiding the fresh catalyst in the laboratory. The baseline catalyst for experiments with these regenerated samples was a fresh catalyst sample which was treated by the same method as the regenerated samples.

All of the aged catalysts were characterized by a number of techniques including quantitative analysis for metals and carbon, BET surface area and desorption pore volume. In addition, the catalyst sample with the greatest age (527 lb SRC/lb catalyst) was subjected to electron microprobe analysis for metals distribution within the catalyst extrudate.

### Pyrene Hydrogenation

The techniques used for the catalytic pyrene hydrogenation reactions and subsequent product analyses have been reported in detail elsewhere (4) and are only briefly described here. Batch reactions were performed (at a temperature of 300°C and nominal hydrogen pressure of 525 psia) in stainless steel microreactors loaded with 100 mg of pyrene, 1 g of hexadecane solvent and 15-19 mg of catalyst. The reactors, which could be rapidly heated to reaction temperature and quenched to ambient temperature at the completion of an experiment, were agitated during the heating period.

Several initial experiments were performed to determine the pressure equilibrium constant for hydrogenation of pyrene to 4,5-dihydropyrene at 300°C and to verify that pseudo first order reversible kinetics accu-

rately modeled the rate of reaction. Following these, hydrogenation experiments for all the fresh, aged and regenerated catalysts were performed in pairs, one experiment with catalyst ground to pass through a 200 mesh sieve (particle diameter 75 μm) to eliminate intraparticle diffusion and the other with whole catalyst extrudates (usually 4-5 per reactor). A nominal weight of 15.4 mg was used for the fresh catalyst. The weights of the aged and regenerated catalysts were increased in proportion to their density to compensate for the weight of contaminants.

Reaction times, which ranged from 10 to 120 minutes, were adjusted according to the activity of the catalysts. Following the completion of an experiment, the products were quantitatively removed from the reactor for analysis by gas-liquid chromatography. In order to determine the ratio of extrudate volume to external surface area, each catalyst extrudate was carefully recovered for measurement of the diameter and length.

## RESULTS

### Catalyst Characterization

Table I lists the results of characterization of the fresh and aged catalysts. As can be seen from Table I, carbon contents increased rapidly during process presulfiding and initial coal-liquids processing, then remained approximately constant after an age of 88 lbs SRC/lb catalyst. However, the amount of contaminant metals, Fe and Ti, continued to increase throughout the run. Catalyst surface areas and pore volumes varied inversely with the carbon contents. Both exhibit a rapid decline during the initial phase of processing followed by nearly constant values after an age of 88 lb SRC/lb catalyst. These trends in amounts of contaminants and physical properties are similar to those found by other investigators of hydroprocessing catalysts (10,11).

Figure 1 shows distribution of the iron and titanium contaminants, determined by electron microprobe analysis, across a circular cross-section of the 527 lb SRC/lb catalyst extrudate (sample 97001). These metals are deposited in an annular shell of the extrudate, a behavior typical of shell progressive pore mouth poisoning.

Figure 2 illustrates the pore volume distribution for fresh Shell 324M and the aged and regenerated 527 lb SRC/lb catalyst sample. As can be seen, the aged catalyst appears to suffer a large loss of pore volume (and related surface area) in the 70 to 140 A diameter pore region. Previous investigators (12,13) have hypothesized that this loss of pore volume and surface area, which is obviously due to the gain in carbon content, is responsible for loss in catalyst activity due to pore blockage with carbonaceous deposits. However, much of the carbonaceous material may simply be trapped reactant and product which is mobile at reaction temperature and does not contribute to pore blockage. Comparison of the curves for the fresh and regenerated catalyst shows that nearly all of the pore volume of the aged catalyst is restored upon removal of the carbonaceous material by regeneration.

### Rate Constants

Results of the initial experiments with ground, freshly presulfided catalyst were used to calculate the pressure equilibrium constant, $1.4 \times 10^{-3}$ $psia^{-1}$, (equation [5]) for reaction [1] at 300°C. Figure 3, a plot of $\ln(X_e/(X_e-X_t))$ vs time for these experiments, demonstrates that the reaction rate follows pseudo first order kinetics. The slope of the linear fit of the data is $k_1 + k_{-1}$ or k of equation [2]. Because $\ln(X_e/(X_e-X_t))$ varies linearly with time and has an intercept of zero, the rate constant may be calculated from the results of a single experiment:

$$k = \ln (x_e/(x_e - x_t))/t \qquad [14]$$

Catalyst Activity and Effective Diffusivity

Fresh Catalyst. The Thiele moduli of the fresh catalysts were calculated from the experimental effectiveness factors ε (ratio of rate constant for the extrudate catalyst to that of the ground, equation [6]) by determining the value of h which satisfied equation [7]. The effective diffusivities were calculated using equation [9] where the ratio of the volume to external surface area is calculated from the average extrudate diameter d and length l:

$$\frac{V_p}{S_x} = \frac{ld^2/4}{d^2/2 + ld} \qquad [15]$$

Regenerated Catalysts. The fraction of catalyst shell poisoned, $\alpha_s$ was given by the ratio of the rate constant for ground regenerated catalyst $k_r$ to that of the ground fresh catalyst $k_f$:

$$\alpha_s = 1 - k_r/k_f \qquad [16]$$

while the fraction F of extrudate activity remaining is the ratio of regenerated extrudate rate constant $k_{re}$ to that of the fresh, $k_{fe}$:

$$F = k_{re}/k_{fe} \qquad [17]$$

Because electron microprobe analysis showed that the contaminant metals were deposited in an annular shell of aged extrudates, it was assumed that the cores of the regenerated catalysts were contaminant free and had activities equal to that of the fresh catalyst. The behavior of F vs $\alpha_s$ for regenerated catalyst, discussed in the next section, supports this assumption. Effective diffusivities for the regenerated catalysts were determined by finding the value $D_e$ which satisfied equation [12]. Note that because $\alpha_c = 0$ for regenerated catalysts, the value of the $k_c$ in equations [12] and [13] is equal to $k_f$.

Aged Catalyst. Calculation of the effective diffusivities for the aged catalysts is similar to that for the regenerated catalyst. Equation [12] is again used; however, the rate constant for the partially deactivated core $k_c$ must be determined from rate constant for the ground aged catalyst experiment $k_{wa}$ and $\alpha_s$ for the corresponding regenerated catalyst

$$k_c = k_{wa}/(1 - \alpha_s) \qquad [18]$$

The fraction of the core which is deactivated $\alpha_c$ is:

$$\alpha_c = 1 - k_c/k_f \qquad [19]$$

and the total fraction deactivated $\alpha_T$ is:

$$\alpha_T = 1 - (k_{wa}/k_f) = \alpha_s + \alpha_c - \alpha_s\alpha_c \qquad [20]$$

Table II lists the rate constants for the ground catalyst and extrudate experiments and Table III gives the fraction poisoned ($\alpha_s$ for the regenerated catalysts and $\alpha_s$, $\alpha_c$ and $\alpha_T$ for the aged catalysts), the fraction F of extrudate activity (compared to fresh extrudate) remaining, the Thiele modulus h, and the effective diffusivity $D_e$.

## DISCUSSION

The results given in Tables II and III can be used to describe the trends in catalyst activity and diffusivity with age and to identify the modes of catalyst deactivation.

Catalyst Activity. Intrinsic catalyst activity, i.e., the activity without diffusion limitations, is given by the rate constants for ground catalyst experiments (Table II). Loss of intrinsic activity is best characterized by the $\alpha$ parameters (Table III). For the regenerated catalysts, the total fraction deactivated, $\alpha_T$, is equal to that due to the metallic contaminants, $\alpha_s$. However, the total fraction deactivated for the aged catalysts is related to the fraction deactivated by carbonaceous deposits $\alpha_c$ and that by metals $\alpha_s$ as given by equation [20]. As can be seen by the values of $\alpha_c$ in Table III, carbonaceous contaminants contribute to a loss of intrinsic catalyst activity of up to 80% during process presulfiding (sample 94074) before processing of coal even begins. However, nearly all of this activity can be recovered by laboratory regeneration methods. After processing of coal begins, metallic contaminants add to the loss in activity and these losses cannot be recovered by regeneration.

Effective Diffusivity. Both the aged and regenerated samples show the same trend in the decrease in effective diffusivities (Table III) with catalyst age. After an initial decrease of ~50% from a value of $6 \times 10^{-6}$ $cm^2/sec/cm^3$ for fresh catalysts to ~$3 \times 10^{-6}$ for catalyst ages greater than 42 lb SRC/lb catalyst, the diffusivity remains relatively constant. Thus, compared to a decrease in intrinsic activity (Table II) of a factor of 30 over the course of the run, a decrease in effective diffusivity of a factor of two appears to have a smaller impact on extrudate activity.

Modes of Deactivation. For the limiting modes of uniform or pore mouth deactivation, equation [12] reduces to equation [10] or [11], respectively. The limiting modes of deactivation may be identified (8) by plotting the fraction of initial extrudate activity remaining after deactivation (F in Table III adjusted by the ratio $\sqrt{\rho De/\rho_f D_{ef}}$) vs the fraction of catalyst deactivated ($\alpha_T$ in Table III). Uniform deactivation behavior, due to the deactivation of catalytic sites homogeneously throughout the extrudate is described by equation [10] which depicts a decrease in activity approximately proportional to $\sqrt{1 - \alpha_T}$. Pore mouth deactivation behavior, which results in an annular shell of deactivation, is described by equation [11] and shows a much different behavior. For pore mouth deactivation, the loss in extrudate activity as a function of fraction deactivated is much greater than that of homogeneous poisoning for the same degree of deactivation.

Because the regenerated catalysts contain only the metallic contaminants, a plot of F vs $\alpha_s$ identifies the mode of deactivation by metals. However, the aged catalysts contain both metallic and carbonaceous contaminants. The plot of F vs $\alpha_T$ for the aged catalysts may identify the dominant mode of deactivation by the deactivating materials.

Figure 4 shows a plot of $F/\sqrt{\rho D_e/\rho_f D_{ef}}$ vs $\alpha_T$ for the regenerated (circles) and aged catalysts (squares). The points for the regenerated samples were accurately fit with the limiting progressive shell pore mouth deactivation model, equation [11], using the average of the Thiele moduli, 5.7, for the samples with significant metals contamination. In contrast, the points for the aged samples were accurately fit with the limiting uniform deactivation model, equation [10], using the average sample Thiele modulus of 2.1. Thus, the catalysts were deactivated by two different modes--progressive shell pore mouth deactivation by metallic contaminants and uniform deactivation by carbonaceous materials. Although the pore mouth mode of deactivation by metals is permanent and limits the amount of extrudate reactivity which can be recovered upon regeneration, the dominant mode of deactivation, which occurs rapidly, is a uniform deactivation by carbonaceous material.

## REFERENCES


1. F. J. Derbyshire and D. D. Whitehurst, Fuel 60, 655 (1981).

2. F. J. Derbyshire, P. Varghese and D. D. Whitehurst, Fuel 61, 859 (1982).

3. B. R. Rogers, R. L. Jolly and R. M. Whan, "ITSL Solvent Quality Studies," Proceedings of the Dept. of Energy Integrated Two-Stage Liquefaction Meeting, Albuquerque, NM, October 1982.

4. H. P. Stephens and R. N. Chapman,"The Kinetics of Catalytic Hydrogenation of Pyrene--Implications for Direct Coal Liquefaction Processing," ACS Fuel Division Preprints, 28, No. 5, 161 (1983).

5. H. P. Stephens in "Coal Liquefaction Process Research Quarterly Report for July 1 - September 30, 1983, Sandia National Laboratories, SAND83-2426, p. 15, January 1984.

6. C. G. Hill, Jr., "An Introduction to Chemical Engineering Kinetics and Reactor Design," John Wiley, NY (1977).

7. R. Aris, Chem. Eng. Sci., 6, 262 (1957).

8. A. Wheeler, Catalysis 2 (105), edited by P. H. Emmett, Reinhold, NY (1955).

9. A. K. Rao, R. S. Pillai, J. M. Lee and T. W. Johnson, "Recent Advances in Two-Stage Coal Liquefaction at Wilsonville," Proceedings of the 8th Annual EPRI Contractors Conference on Coal Liquefaction, EPRI AP-3366-SR, February 1984.

10. G. J. Stiegel, R. E. Tischer and D. L. Cillo, "Catalyst Testing for Two-Stage Liquefaction," Proceedings of the 8th Annual EPRI Contractors Conference on Coal Liquefaction, EPRI AP-3366-SR, February 1984.

11. R. Galiasso, R. Blanco, C. Gonzales and N. Quinteros, Fuel 62, 817 (1983).

12. M. J. Chiou and J. H. Olson, ACS Symp. Ser. 23, 1421 (1978).

13. B. D. Prasher, G. A. Gabriel and Y. H. Ma, Ind. Eng. Chem. Process Des. Dev. 17, 266 (1978).

Table I. Elemental Analysis, Surface Areas and Pore Volumes for the Fresh and Aged Catalysts

| Sample | Age (lb feed/lb catalyst) | Active Metals (Wt %) Mo | Ni | Major Contaminants (Wt %) C | Fe | Ti | Surface Area ($m^2/g$) | Pore Volume (cc/g) |
|---|---|---|---|---|---|---|---|---|
| Fresh | -- | 12.4 | 2.8 | 0.11 | .02 | .07 | 158 | 0.49 |
| 15923 | Process Presulfided | NA | NA | 2.33 | NA | NA | 142 | 0.41 |
| 97888 | Process Presulfided | NA | NA | 4.40 | NA | NA | 137 | 0.38 |
| 94074 | Process Presulfided | 10.3 | 2.3 | 6.1 | .04 | .14 | 135 | 0.35 |
| 94495 | 43 | 10.3 | 2.3 | 8.2 | .14 | .14 | 125 | 0.32 |
| 94811 | 88 | 10.0 | 2.2 | 9.3 | .22 | .21 | 113 | 0.29 |
| 94966 | 133 | 10.1 | 2.4 | 9.6 | .28 | .30 | 108 | 0.28 |
| 96460 | 381 | 9.5 | 2.5 | 9.2 | .67 | .46 | 102 | 0.27 |
| 97001 | 527 | 9.7 | 2.4 | 9.4 | .72 | .56 | 100 | 0.27 |

Table II. Weight Basis Rate Constants for Ground Catalyst and Extrudate Experiments

| Sample | Age (lb/lb) | Aged Catalyst Rate Constants ($sec^{-1}$ $g^{-1}$x$10^2$) Ground | Extrudate | Regenerated Catalyst Rate constants ($sec^{-1}$ $g^{-1}$x$10^2$) Ground | Extrudate |
|---|---|---|---|---|---|
| Fresh | -- | 15.9 | 4.1 | 17.6 | 4.7 |
| 15923 | Process Presulfided | 8.9 | 3.3 | 17.6 | 5.0 |
| 97888 | Process Presulfided | 3.4 | 1.5 | 17.2 | 4.3 |
| 94074 | Process Presulfided | 2.3 | 0.99 | 16.8 | 3.8 |
| 94495 | 43 | 1.6 | 0.39 | 13.6 | 1.3 |
| 94811 | 88 | 1.2 | 0.59 | 12.1 | 1.7 |
| 94966 | 133 | 0.88 | 0.37 | 11.8 | 0.98 |
| 96460 | 381 | 0.49 | 0.32 | 7.2 | 0.85 |
| 97001 | 527 | 0.49 | 0.26 | 5.2 | 0.45 |

Table III. Fractions Poisoned, $\alpha$, Fraction Extrudate Reactivity Remaining, F, Thiele Modulus, h, and Effective Diffusivities, De, for Fresh, Aged, and Regenerated Catalysts.

| | Aged Catalysts | | | | | | Regenerated Catalysts | | | |
|---|---|---|---|---|---|---|---|---|---|---|
| Sample | $\alpha_T$ | $\alpha_S$ | $\alpha_C$ | F | h | De$10^6$ | $\alpha_S$ | F | h | De$10^6$* |
| Fresh | -- | -- | -- | 1.0 | 3.8 | 5.6 | -- | 1.0 | 3.7 | 6.2 |
| 15923 | .44 | .003 | .44 | .81 | 2.5 | 6.7 | .003 | 1.06 | 3.5 | 6.3 |
| 97888 | .77 | .02 | .77 | .39 | 2.1 | 4.2 | .02 | .92 | 3.8 | 6.0 |
| 94074 | .84 | .04 | .84 | .26 | 2.1 | 2.9 | .04 | .80 | 4.2 | 5.4 |
| 94495 | .89 | .22 | .85 | .11 | 3.1 | 1.3 | .22 | .28 | 5.9 | 2.6 |
| 94811 | .92 | .30 | .88 | .16 | 1.6 | 3.7 | .30 | .35 | 4.6 | 4.5 |
| 94966 | .93 | .30 | .91 | .11 | 1.9 | 2.0 | .30 | .22 | 6.2 | 2.3 |
| 96460 | .96 | .57 | .92 | .09 | 1.3 | 4.2 | .57 | .19 | 5.0 | 3.4 |
| 97001 | .96 | .68 | .88 | .08 | 1.8 | 2.9 | .68 | .10 | 6.9 | 2.1 |

*De has units of $cm^2/sec/cm^3$.

FIGURE 1. Distribution of Fe and Ti across a circular cross-section of extrudate sample 97001, aged 527 lbs SRC/lb catalyst.

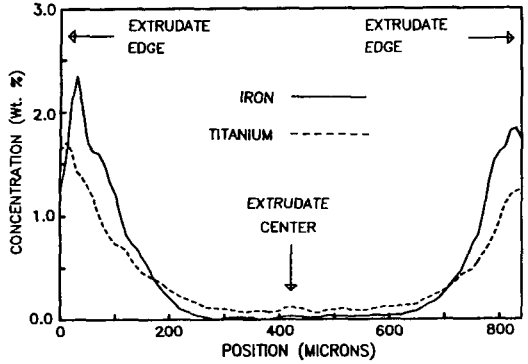


FIGURE 2. Pore volume distribution for fresh catalyst, oged, and regenerated sample 97001.

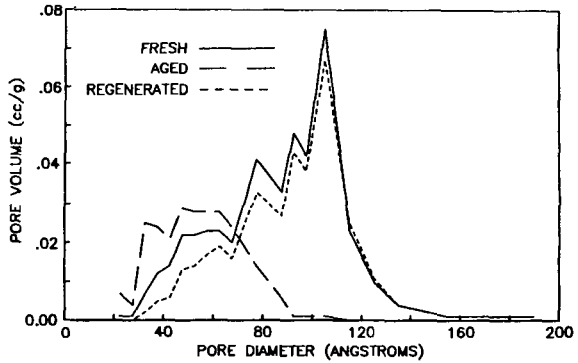


FIGURE 3. Plot of pseudo first order reversible reaction kinetics for hydrogenation of pyrene to 4,5-dihydropyrene.

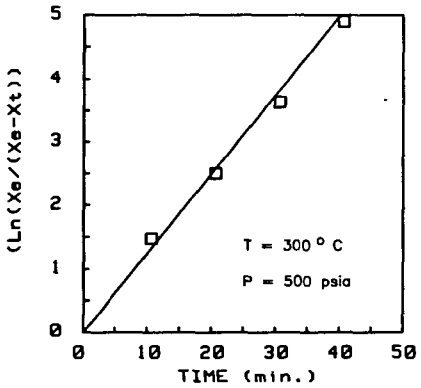


FIGURE 4. Plot of fraction extrudate activity remaining vs total fraction deactivated for aged and regenerated extrudates.

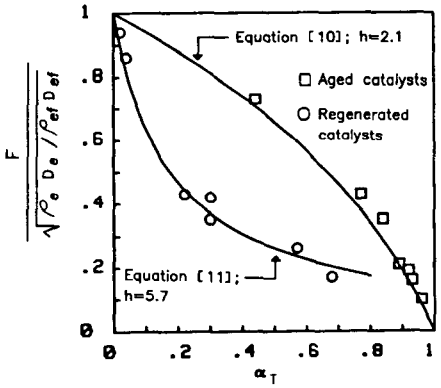

# A CATALYTIC REACTION MODEL FOR FILAMENTOUS CARBON GASIFICATION

J. A. Starkovich, Wei-Yue Lim, H. Peng

Chemical Processes Department, TRW Energy Development Group,
Redondo Beach, California 90278

## 1. Introduction

Filamentous coke deposition is a major fouling problem for catalysts used in synthesis gas methanation, the water-gas shift reaction and hydrocarbon steam reforming. Significant effort has been spent in studying carbon deposition rate, deposit morphology and structure, and process conditions for minimization of deposition rate. A collection of papers from a special symposium and an excellent review article which survey this work have recently appeared. (1,2) Much less study, however, has been devoted to modeling the inverse reaction or the gasification/removal of filamentous carbon deposits. Information and fundamental understanding of the kinetics of the inverse reaction are needed for improved design of catalyst regeneration schemes used in commercial catalytic fuel gas processing. Better understanding of the inverse reaction may also assist identification of improved deposit prevention methods.

The present research was undertaken to develop a model for correlating conversion rate with the extent of conversion for the gasification of filamentous carbon. In our studies of the gasification reactions of filamentous carbon, we find that traditional fluid-solid reaction models such as the "shrinking core", shrinking sphere" and progressive conversion, are not adequate for describing conversion kinetics. We suspect from our work and the results of others (3,4,5) that certain filamentous carbon gasification reactions proceed via a catalytic mechanism involving an embedded catalyst particle. We have developed a new model for this type of reaction which we have termed the "axially shrinking filament" model. The conceptual basis and formulation for this new model are presented in this paper. Refinement and experimental verification/application of this new model are in progress. An illustrative example of the model's ability for describing the conversion kinetics of the filamentous carbon-hydrogen reaction is presented from this work.

## 2. Axially Shrinking Filament Model

Essential features of the axially shrinking filament (ASF) model are illustrated in Figure 1. As depicted, the solid grain consists of a consumable filament-shaped particle attached to a small catalyst nodule. For a grain situated in a fluid reactant medium, the catalyst nodule serves as the site of reaction between fluid reactant and the filament particle. In reaction, fluid reactant is adsorbed by the catalyst nodule and combines with filament material in the vicinity of the nodule. The initially formed reaction product is subsequently desorbed and lost to the bulk fluid phase. Continuing reaction and loss of filament material results in axial shrinkage of the grain without change in filament cross-section. The rate of the topochemical reaction is constant throughout conversion of an individual filament and is proportional to the interfacial area between the nodule and filament. Different diameter filaments thus exhibit the same linear shrinkage rate, v, under a given set of reaction conditions. The shrinkage observed for each filament in a collection of reacting grains is given by vt, where t

is the reaction time. The shrinkage rate may be a function of temperature, reactant, nodule composition and orientation, and possibly other physiochemical conditions of the reaction. Interphase heat and mass transport resistances, if significant, are assumed to be constant during reaction.

A global conversion expression may be developed for this reaction model by considering the particle collection to have a time-dependent filament length distribution. Change in filament length distribution due to reaction is related to conversion extent or in the present case, the amount of carbon gasified. A general expression for relating fractional conversion, $\alpha$, to the filament length distribution is given by Equation (1). The terms $l$ and $p_o\{l\}$ are the filament length and the fraction of the initial ($t=o$) population having length $l$. $p_o\{l\}$ is the probability density function or the length distribution function for the particle collection and may be considered a continuous function of $l$ for large number filament populations.

$$\alpha = 1 - \frac{\int_{vt}^{\infty} l\,p_o\{l\}\,dl - vt\int_{vt}^{\infty} p_o\{l\}\,dl}{\int_{o}^{\infty} l\,p_o\{l\}\,dl} \qquad 1)$$

While the derivation of this expression is being presented elsewhere, the intuitive correctness of the expression may be appreciated by pointing out the essence of the integral terms. The entire ratio on the right-hand side of Equation (1) is the mass fraction of carbon remaining at time t. The denominator integral simply represents the average filament length for the particle collection before any reaction (t=0). The numerator is the difference between the average length of that portion of the initial filament population with a length equal to or greater than vt and the total shrinkage length suffered by this population segment up to time t. It is important to note that Equation (1) is a general conversion expression independent of filament geometry and is valid for any continuous probability density function. In order for the equation to be useful in practice, the distribution function must be known a priori from independent measurement or ascertained from a gasification experiment. Application of Equation (1) for describing the gasification of filamentous carbon is shown below.

## 3. Experimental

Filamentous carbons used in these studies were prepared by carbon monoxide disproportionation over cobaltosic oxide. Cobaltosic oxide is an active CO disproportionation catalyst and produces filamentous carbon as the principal deposit form at temperatures below approximately 873°K. In the preparation, heated carburizing gas mixture is flowed over a sample of thinly-dispersed, fine oxide powder. Deposition is carried out until the deposit solid contains approximately 90-95 wt. percent carbon. A $CO-H_2$ mixture (85:15 mole ratio) is used for the carburizing gas and the deposition temperature is maintained at 723°K. These conditions lead to the production of filaments with diameters in the range of 50-200 nm and large apparent length-to-diameter ratios when examined by scanning and transmission electron microscopy.

Reaction of a filamentous carbon sample with hydrogen was conducted

using a differential, micro-packed bed reactor system. In a typical gasification experiment, hydrogen of a constant flowrate is passed through a loosely-packed 1 gram sample of filamentous carbon and the flowrate and composition of exit gas measured as a function of time. Hydrogen and methane content of the exit gas is measured by an automatic sampling gas chromatograph. Exit flowrate is measured and recorded by a custom-designed volumetric displacement type flowmeter. The precision and accuracy of all measurements permitted carbon mass balances for test reactions of 96-102% to be routinely obtained. All reactions were conducted at near atmospheric pressure over the temperature range from 798 to 1073°K. Commercially pure bottled hydrogen and deuterium were used in all reactions. Further description of the reactor system and experimental procedures is being reported elsewhere.

## 4. Results and Discussion

Representative gasification curves for filamentous carbon are shown in Figure 2. For the temperature range investigated, all reactions displayed a similarly shaped conversion curve. During the initial 60-70% carbon gasification, the global rate for all reactions was virtually constant, exhibiting a zero-order dependence on carbon. Beyond approximately 70% conversion, reaction rate declined rapidly with further conversion. The zero-order rate dependence is consistent with a catalytic or topochemical reaction involving axial attack of long length filaments. The reaction span marked by an unsteady rate probably has zero-order rate dependence also, but this is masked by a diminishing percentage of reacting filaments. The zero-order dependence observation agrees with observations made in other studies [4,5] involving carbons produced from hydrocarbons and employing different deposition catalysts. The activation energy determined for the gasification reaction below 873°K is approximately 178 KJ/mole. Between approximately 873 and 1023°K an apparent maximum in reaction rate was observed. This maximum, however, was an experimental artifact due to the attainment of equilibrium and the onset of hydrogen feedrate control of the reaction.

The ability of the ASF model to quantitatively fit experimental data is illustrated in Figure 3. This correlation was made using the Gaussian normal probability function [6] for the filament length distribution term in Equation (1) and using non-linear least squares regression analysis to determine the model parameters. The integral expression used for regression is given in Equation (2). The terms $\bar{l}_o$ and $\sigma^2$ used in this equation refer to the filament length distribution parameters, mean length, and variance for the initially unreacted sample. Selection of the Gaussian function to represent the filament length distribution is a reasonable choice in the absence of any foreknowledge about the length distribution. It is intermediate between a monodisperse and uniform length distribution in its effect on the predicted shape of the gasification curve. Additionally, it requires only two parameters, a mean and variance, to fully describe the distribution.

$$\alpha = 1 - \frac{\int_{vt}^{\infty} l \exp\left\{-\tfrac{1}{2}\left(\frac{l-\bar{l}_o}{\sigma}\right)^2\right\} dl - vt \int_{vt}^{\infty} \exp\left\{-\tfrac{1}{2}\left(\frac{l-\bar{l}_o}{\sigma}\right)^2\right\} dl}{\int_{0}^{\infty} l \exp\left\{-\tfrac{1}{2}\left(\frac{l-\bar{l}_o}{\sigma}\right)^2\right\} dl} \qquad 2)$$

As indicated by Figure 2 the model appears adequately capable of describing the conversion kinetics of filamentous carbon. Appropriateness of the ASF model was further evaluated in a special series of tests. In this series, samples of carbon produced from a single deposition experiment were reacted at different temperatures and model parameters determined for each reaction. If the model is an appropriate one, only the filament shrinkage rate, v, should be observed to vary with temperature; the filament length distribution parameters should be constant within sampling and experimental error. That this is indeed the case may be seen from the results presented in Table 1. While v increases by nearly a factor of five in going from a reaction temperature of 798 to 848°K, $\bar{l}_o$ and $\sigma$ remain relatively constant. Increasing the reaction temperature to 1073°K, where there is a definite change in Arrhenius activation energy, and also switching to deuterium reactant yield the same distribution parameter values. This is further evidence of the appropriateness of the model. The ASF model is a macro-physical description of the reaction and is not based on any particular, molecular rate-controlling mechanism.

Table 1. Regression fitted model parameters for various temperature reactions.

| Gasification Temperature, °K | Model Parameter | | |
|---|---|---|---|
| | v[a] | $\bar{l}_o$[b] | $\sigma$ |
| 798 | .39 | 84 | 16 |
| 823 | 1.00 | 84 | 15 |
| 848 | 1.91 | 82 | 22 |
| 1073 | 0.80 | 83 | 20 |
| 1073 | 0.81[c] | 82[c] | 26[c] |
| | Average | 83 | 20 |

a Filament shrinkage rate relative to 823°K value.

b Filament distribution average length and standard deviation expressed in dimensionless length units.

c Results for deuterium - carbon gasification reaction.

## 5. Summary and Conclusions

A general reaction model has been proposed for describing the gasification of filamentous carbons. The model, termed the "axially shrinking filament" model, successfully correlates gasification data obtained for the hydrogen-filamentous carbon reaction where the carbon is produced from CO disproportionation over a cobalt catalyst. The model may be applicable for other filamentous carbon gasification reactions and should be useful in the design of coked catalyst regeneration schemes.

## REFERENCES


1. Albright, L. F., Baker, R. T. K. eds Coke Formation on Metal Surfaces, American Chemical Society Symposium Series 202, ACS, Wash, D.C., 1982.

2. Baker, R. T. K., Harris, P. S., The Formation of Filamentous Carbon, in Chemistry and Physics of Carbon, Vol. 14, P. L. Walker, P. A. Thrower eds., 83-165, 1978.

3. Figueiredo, J. L., Trimm, D. L., J. Catal. (1975), 40, 154.

4. Nishiyama, Y., Tamai, Y., Carbon (1976), 14, 13.

5. Figueiredo, J. L., Carbon (1981), 19, 146.

6. Abramowitz, M., Stegun, I. A., eds, Handbook of Mathematical Functions, Dover Publications, N.Y., 1965.


FIGURE 1. AXIALLY SHRINKING FILAMENT MODEL.

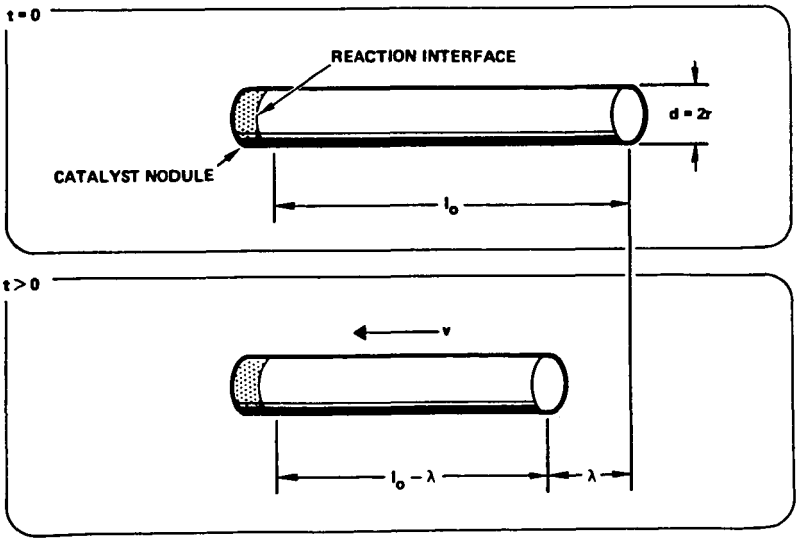

FIGURE 2. REPRESENTATIVE CONVERSION-TIME CURVES FOR FILAMENTOUS CARBON GASIFICATION.

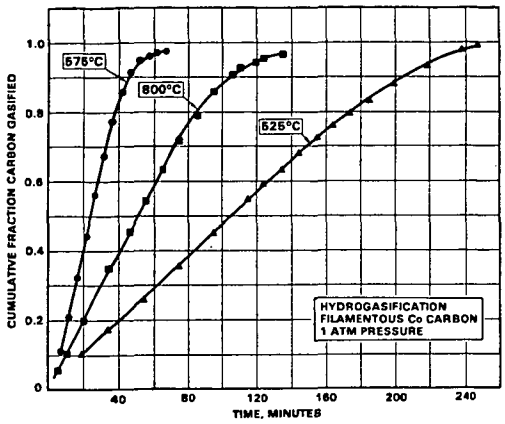


FIGURE 3. MODEL CORRELATED REACTION DATA FOR FILAMENTOUS CARBON GASIFICATION.

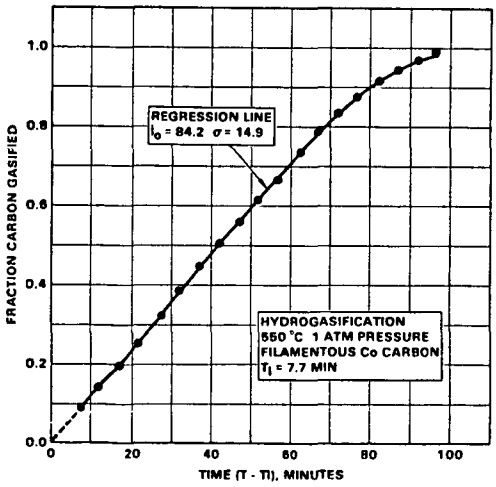

# Metal Particle Characterization of Zeolite-Based Syngas Conversion Catalysts

V.U.S. Rao, R.T. Obermyer,* A. Shamsi, R.K. Wicker,**
R.J. Gormley and R.R. Schehl

U.S. Department of Energy
Pittsburgh Energy Technology Center
P.O. Box 10940, Pittsburgh, PA 15236,

*Department of Physics, Pennsylvania State University
McKeesport, PA 15132, and

**Washington and Jefferson College, Washington, PA 15301

## INTRODUCTION

The conversion of $CO+H_2$ in one step to a mixture of hydrocarbon species that are the constituents of high octane gasoline appears possible with catalysts composed of ZSM-5 and a group VIII metal (1-5). The group VIII metal acts as a Fischer-Tropsch (F-T) catalyst and converts synthesis gas to a mixture of olefins, paraffins, and oxygenates. The ZSM-5 component of the catalyst converts some of the F-T intermediates and products to aromatics and branched-hydrocarbon species.

The present study attempts to characterize the metal crystallite size and the degree of reduction of cobalt-ZSM-5 catalysts using chemisorption and magnetization measurements. The catalysts prepared by the solution-impregnation method were examined. It was realized that the method could result in partial ion exchange of the acidic protons in ZSM-5 with cobalt ions (5-7). The ion-exchanged cobalt ($Co^{2+}$) is catalytically inactive in synthesis gas conversion (6,7), since it cannot be reduced to metallic cobalt under usual reduction treatment, namely, flowing hydrogen at 350°C. The present study attempts to demonstrate how chemisorption and magnetization measurements on Co/ZSM-5 catalysts with different Co concentrations can enable one to estimate the weight percent Co that has been ion-exchanged into ZSM-5.

It has been reported (8,9) that ($Fe^{2+}$, $NH_4^+$)Y can react with an anionic, metal-containing coordination compound that is water-soluble, such as $(NH_4)_3[Fe(CN)_6]$, to yield an insoluble compound, $Fe_3[Fe(CN)_6]_2$, distributed throughout the zeolite while the zeolite itself returns to the ammonium form. The insoluble complex can later be reduced in hydrogen to finely dispersed metal in the zeolite (9). The present work attempts to examine whether the above method could be used to convert ion-exchanged $Co^{2+}$ in ZSM-5 to a reducible and catalytically active form. Since it was of interest to examine the catalytic activities of both the metal component and the zeolite component, before and after the reaction with the coordination compound, separate experiments were performed with syngas and ethylene as the reactants. Syngas conversion is primarily catalyzed by the metal component; and ethylene conversion, by the zeolite component in the catalyst.

## EXPERIMENTAL

### (a) Preparation of Catalysts

The ZSM-5, with $SiO_2/Al_2O_3 \sim 30$, was synthesized using the procedure given in the patent literature by Argauer and Landolt (10), with minor modifications. The procedure yields ZSM-5 having crystallites approximately one micron in size. The zeolite was calcined in air at 538°C to decompose the tetrapropylammonium ($TPA^+$)

cation. It was converted to the ammonium form by three successive exchanges using $NH_4Cl$ solution.

To prepare the metal-loaded catalysts, the solution-impregnated method was used. Aqueous cobalt (II) nitrate solution was added to $NH_4$-ZSM-5 until incipient wetness was reached. The atmosphere surrounding the mixture was evacuated after the solution was added. The mixture was dried with stirring at 100°C. Three samples with 2.7, 5.9, and 9.0 wt% Co/$NH_4$-ZSM-5 were prepared by this method.

In order to prepare a sample of Co/$NH_4$-ZSM-5 in which the cobalt could be expected to be almost entirely in the ion-exchanged form, the following procedure was used. Ten grams of $NH_4$-ZSM-5 was added to 120 mL of 9.5 wt% $Co(NO)_3 \cdot 6H_2O$ solution in water at 90°C. The mixture was stirred for one hour and filtered. The procedure was repeated two more times, and the zeolite sample was thoroughly washed with water until no nitrate was present. The sample had 0.9 wt% Co, presumably in the ion-exchanged form (IE), and will be designated 0.9 wt% Co/$NH_4$-ZSM-5 (IE).

"Back-exchange" (BE), i.e., removal of the ion-exchanged $Co^{2+}$ from the zeolite, was attempted on the basis of the following reaction (8):

$$Co^{2+}\text{-Z} + (NH_4)_4[Fe(CN)_6] \rightarrow NH_4\text{-Z} + Co_2[Fe(CN)_6]$$

The $Co_2[Fe(CN)_6]$, an insoluble compound, would be distributed throughout the zeolite. Subsequent reduction in hydrogen at 400°C should result in a zeolite containing cobalt and iron, while the zeolite itself is converted to the H-form.

To carry out the back-exchange, 15 g of 0.9 wt% Co/$NH_4$-ZSM-5 (IE) was stirred in 150 mL of 3.3 wt% $(NH_4)_4Fe(CN)_6 \cdot H_2O$ solution in water for 4 hours at room temperature. The mixture was filtered. The back-exchanged zeolite sample was analyzed and found to contain 0.9 wt% Co and 0.2 wt% Fe, and will be designated 0.9 wt% Co, 0.2 wt% Fe/$NH_4$-ZSM-5 (BE).

A part of each of the five samples was pelleted into 3-mm-diameter tablets for catalytic activity tests. The pellets were calcined in air at 450°C for one hour to convert the $NH_4$-ZSM-5 to the H-form. Parallel studies using infrared spectroscopy showed deammoniation was nearly complete under these conditions (7).

(b) Magnetization Measurements

Samples for magnetic analysis were placed in 4-mm-outside-diameter glass tubes and reduced in flowing hydrogen at 350°C for 16 hours. The tubes were then sealed under vacuum.

The magnetic measurements were performed using a vibrating sample magnetometer in applied fields up to 15 kOe. The saturation magnetization was obtained by plotting $\sigma$ versus 1/H and extrapolating to zero (infinite fields). The values obtained were compared with the known saturation magnetization of bulk metallic cobalt, and the degree of reduction was obtained. The percent reduction is reported in Table I.

(c) Chemisorption Measurements

Hydrogen adsorption measurements were performed using a conventional glass volumetric adsorption apparatus. One gram of catalyst sample was used. The sample was heated to 200°C (4°C/min) under flowing He (60 mL/min) and kept at that temperature for 1 hour. The sample chamber was evacuated and cooled to 50°C. Hydrogen (60 mL/min) was introduced and the temperature was raised to 350°C (4°C/min). The sample was reduced at 350°C for 16 hours. The sample chamber was evacuated to $10^{-5}$ torr and cooled to the adsorption temperature.

The $H_2$ adsorption measurements were conducted at 100°C. The adsorption isotherms are shown in Figure 1.

(d) Metal Particle Size Calculations

The values of hydrogen uptake were extrapolated to zero hydrogen pressure from the linear portion of the isotherm (Figure 1), as outlined by other workers for nickel catalysts (11,12).

The metal dispersions $D=Co_s/Co_t$, where $Co_s$ is the number of surface cobalt atoms and $Co_t$ is the total number of cobalt atoms, were calculated using the adsorption stoichiometry of $H/Co_s=1$. Average crystallite diameters (Table I) were calculated from %D for spherical hcp metal crystallites (6) of uniform diameter using the following relation (13):

$$d(nm) = 73.81/\%D$$

(e) Catalytic Conversion Tests

The equipment used was a downflow, fixed bed reactor of 1-cm inner diameter. The mass of the catalyst sample was 1.35 g. The sample was reduced in hydrogen at 350°C. The conversion of syngas ($H_2/CO=1$) at 280°C, 12 bar, and a flow of 0.659 g/g cat. hr was examined for a 24-hour period.

The products of the reaction were $CO_2$, $H_2O$ and hydrocarbons, and were analyzed using gas chromatography. The $C_5+$ product was analyzed using simulated distillation. It was also separated into aromatics, olefins and saturates using the FIA method.

Ethylene conversion studies were also conducted in a reactor similar to that mentioned above. After treatment with hydrogen at 350°C, the reaction mixture consisting of 30 vol% $C_2H_4$ and 70 vol% $H_2$, was introduced at 1 atm and a flow rate of 0.983 g/g cat. hr. The temperature of the reactor was maintained at 320°C. The products were analyzed as described above.

## RESULTS AND DISCUSSION

The results of magnetization and chemisorption studies are shown in Table I, Figure 1, and Figure 2. For the three catalysts containing 9.0, 5.9, and 2.7 wt% Co, approximately 2.2 wt% of the catalyst is the amount of cobalt that has not been reduced to metallic cobalt in flowing hydrogen at 350°C (see Table I). The hydrogen uptake and the degree of reduction exhibit similar trends when plotted against the cobalt loading (Figure 2), and each curve intercepts the horizontal axis at nearly 2.2 wt%.

The amount of hydrogen chemisorbed can be expected to be approximately proportional to the metal surface area. The absence of metallic cobalt in a sample would result in zero chemisorption of hydrogen. It is thus understandable that both the hydrogen uptake and the degree of reduction obtained from the magnetization study become vanishingly small at the same concentration (2.2 wt%) of cobalt in the catalyst.

The results from $H_2+CO$ conversion experiments are shown in Figure 2 and Table II. The variation of the rate of conversion with cobalt loading also follows the same trend as the chemisorption and degree of reduction. Of the liquid hydrocarbon products obtained with these catalysts, nearly 95% is in the gasoline boiling range, as revealed by simulated distillation. The $C_5+$ product consists of aromatics, branched olefins, and branched paraffins, which are constituents of high octane gasoline.

The conversion of $H_2$+CO by 0.9 wt% Co/ZSM-5 (IE) is zero, consistent with the observation that the degree of reduction is zero after exposure to hydrogen at 350°C (Table I and Figure 2). This provides additional support that the cobalt in this sample is in an ion-exchanged form that cannot be reduced to the catalytically active metallic cobalt. When the sample is back-exchanged to yield 0.9 wt% Co, 0.2 wt% Fe/ZSM-5 (BE), the CO+$H_2$ conversion is 17.3%, and the degree of reduction is 48%. The existence of a ferromagnetic moment indicates that Co (and possibly Fe) is in the metallic state in the back-exchanged sample.

The conversion of ethylene over H-ZSM-5 and the metal-zeolite samples (ion-exchanged and back-exchanged) was used as a method for comparison of their catalytic acid function. The results are shown in Table III for the first six hours on stream. The cobalt-exchanged sample exhibits $C_2H_4$ conversion of 78.7%, while the H-ZSM-5 (parent sample) exhibits a conversion of 86.1%. The cobalt-exchanged sample also yields a lower fraction of aromatics (37%) in comparison to H-ZSM-5, which yields 53% aromatics in the liquid hydrocarbon product. It is thus indicated that the acid function of the zeolite is weakened by the presence of cobalt in ion-exchanged form. Back-exchange of the cobalt results in a catalyst that brings about an improved ethylene conversion (89.8%) and larger aromatic fraction (42%).

The above results obtained from physical measurements (chemisorption and magnetization) and catalytic activity tests indicate how metal speciation in cobalt/ZSM-5 can be characterized. The parent sample of H-ZSM-5 with $SiO_2/Al_2O_3$=38 can be represented by

$$H^+_{0.050} \left( Si_{0.950} \, Al_{0.050} \, O_2 \right)^{-0.050}$$

The ion-exchanged sample 0.9 wt% Co/ZSM-5 (IE) can be represented by

$$H^+_{0.028} \, Co^{2+}_{0.011} \left( Si_{0.950} \, Al_{0.050} \, O_2 \right)^{-0.050}$$

It can be noticed that 44% of the $H^+$ sites have been exchanged with cobalt, resulting in weakened acidity. In the back-exchanged sample, at least 48% of $Co^{2+}$ has been replaced by $NH_4^+$, while the cobalt is converted to the insoluble compound $Co_2\left[Fe(CN)_6\right]$. Calcination at 450°C, followed by reduction in $H_2$ at 350°C, results in the conversion of the zeolite to the $H^+$-form and the formation of metallic cobalt. The resulting sample exhibits catalytic activity for synthesis gas conversion.

## CONCLUDING REMARKS

This study demonstrated that magnetic and chemisorptive techniques can be used to characterize metal speciation in catalysts such as Co/ZSM-5. In particular, the amounts of ion-exchanged cobalt and cobalt external to the zeolite can be estimated. These measurements enable one to intepret the catalytic activity and selectivity of the catalyst.

In our attempts to introduce cobalt in cationic form in ZSM-5 a temperature of 90°C has been used for the exchange with aqueous cobalt nitrate solution. It appears that 0.9 wt% Co can be introduced into ZSM-5 of $SiO_2/Al_2O_3$=38 under these circumstances. Analyses of the Co/ZSM-5 samples that were prepared by impregnation at room temperature with cobalt nitrate solution showed that approximately 2.2 wt% Co was in a form not reducible to metallic cobalt (Table I). In earlier work (6,7), the Co/ZSM-5 samples were subsequently washed with water to yield samples that contained 1.4-1.7 wt% Co. Hence it is possible that exchange at temperatures lower than 90°C would yield samples containing more than 0.9 wt% Co in ion-exchanged form (14).

This study has shown that $Co^{2+}$/ZSM-5 can be back-exchanged and reduced to yield metallic cobalt supported on H-ZSM-5. Chemisorption measurements are currently being carried out to determine the degree of dispersion of such samples. The back-exchanged samples are catalytically active in synthesis gas conversion. The method of back-exchange should be generally applicable for preparing metal-zeolite catalysts where it is desirable to free the zeolite of metal cations in order to restore the acidity to its original strength, and to have the metal on the exterior of the zeolite crystallites in a highly dispersed, catalytically active form.

ACKNOWLEDGMENTS

The authors would like to thank Bernard D. Blaustein, John M. Stencel, and Kee H. Rhee for helpful discussions.

REFERENCES

1. C.D. Chang, W.H. Lang, and A.J. Silvestri, J. Catal. 56, 268 (1979).
2. P.D. Caesar, J.A. Brennan, W.E. Garwood, and J. Ciric, J. Catal. 56, 274 (1979).
3. V.U.S. Rao and R.J. Gormley, Hydrocarbon Process., 59(11), 139 (1980).
4. T.J. Huang and W.O. Haag, ACS Symposium Series 152, 308 (1981).
5. V.U.S. Rao, Physica Scripta T4, 71 (1983).
6. J.M. Stencel, V.U.S. Rao, J.R. Diehl, K.H. Rhee, A.G. Dhere, and R.J. DeAngelis, J. Catal. 84, 109 (1983).
7. V.U.S. Rao, R.J. Gormley, R.R. Schehl, K.H. Rhee, R.D.H. Chi, and G. Pantages, in "Catalytic Conversions of Synthesis Gas and Alcohols to Chemicals," Ed. R.G. Herman, Plenum (1984), p. 151.
8. J. Scherzer and D. Fort, J. Catal. 71, 111 (1981).
9. J. Scherzer, J. Catal. 80, 465 (1983).
10. R.J. Argauer and G.R. Landolt, U.S. Patent 3,702,886 (1972), Example 24.
11. M.A. Vannice and R.L. Garten, J. Catal. 56, 236 (1979).
12. C.H. Bartholomew and R.B. Pannell, J. Catal. 65, 390 (1980).
13. R.C. Reuel and C.H. Bartholomew, J. Catal. 85, 63 (1984).
14. P. Chu and F.G. Dwyer, ACS Symp. Series 218, 59 (1983).

TABLE I

Results from Magnetization and Chemisorption on Co/ZSM-5

| Metal Loading (wt%) | % Reduction in $H_2$ at 350°C (from magnetization) | Wt% Co Unreduced | $H_2$ Uptake at 100°C ($\mu$ mol $g^{-1}$) | d(nm) |
|---|---|---|---|---|
| 9.0 | 78 | 2.0 | 35.4 | 12.4 |
| 5.9 | 64 | 2.1 | 22.5 | 10.4 |
| 2.7 | 10 | 2.5 | 2.4 | 8.5 |
| 0.9 (IE) | 0 | 0.9 | | |
| 0.9 (BE) +0.2 Fe | 48 | 0.4 | | |

TABLE II

Conversion and Product Distribution From Co/ZSM-5 Catalysts
During the Initial 24-Hour Period
IE: ion-exchanged; BE: back-exchanged

$H_2/CO$ = 1; P = 21 bar; Temperature = 280°C; Feed Rate = 0.659 g/g cat. hr

| Co in Catalyst (wt%) | 9.0 | 5.9 | 2.7 | 0.9 (IE) | 0.9 (BE) +0.2 Fe |
|---|---|---|---|---|---|
| CO Conversion (%) | 56.5 | 54.6 | 21.0 | 0.0 | 13.7 |
| $H_2$ Conversion (%) | 85.8 | 80.8 | 34.3 | 0.0 | 20.9 |
| $CO+H_2$ Conversion (%) | 70.7 | 67.3 | 27.4 | 0.0 | 17.3 |
| Product Composition (wt%) | | | | | |
| $CO_2$ | 18.6 | 13.2 | 8.1 | | 13.9 |
| $H_2O$ | 46.1 | 50.9 | 56.6 | | 55.9 |
| $CH_n$ | 35.2 | 35.8 | 35.3 | | 30.2 |
| Composition of $CH_n$ (wt%) | | | | | |
| $CH_4$ | 24.4 | 24.0 | 33.6 | | 42.4 |
| $C_2H_4$ | 0.0 | 0.4 | 0.0 | | 0.0 |
| $C_2H_6$ | 2.7 | 2.3 | 5.2 | | 3.1 |
| $C_3H_6$ | 0.8 | 0.6 | 0.0 | | 0.0 |
| $C_3H_8$ | 2.7 | 2.7 | 7.7 | | 18.4 |
| $C_4H_8$ | 0.8 | 1.4 | 0.9 | | 0.0 |
| $C_4H_{10}$ | 5.4 | 6.6 | 18.7 | | 24.2 |
| $C_5+$ | 63.0 | 61.9 | 33.8 | | 11.8 |
| Liquid Product Composition (vol%) | | | | | |
| Aromatics | 19.5 | 23.0 | | | |
| Olefins | 32.5 | 30.5 | | | |
| Saturates | 48.0 | 46.5 | | | |

TABLE III

Conversion of 30 vol% $C_2H_4$ + 70 vol% $H_2$ Mixture over H-ZSM-5 and Co/ZSM-5 ($SiO_2/Al_2O_3$=38).

Feed Rate = 0.983 g/g cat. hr; Temperature = 320°C

| Catalyst | H-ZSM-5 | 0.9% Co/H-ZSM-5 (ion-exchanged) | 0.9% Co, 0.2% Fe/H-ZSM-5 (back-exchanged) |
|---|---|---|---|
| Period (hours) | 0-6 | 0-6 | 0-6 |
| $C_2H_4$ Conversion (%) | 86.1 | 78.7 | 89.8 |
| $H_2$ Conversion (%) | 9.2 | 8.5 | 13.4 |
| Product Composition (wt%) | | | |
| $CH_4$ | 0.0 | 0.0 | 0.0 |
| $C_2H_6$ | 14.5 | 13.3 | 27.0 |
| $C_3H_6$ | 7.6 | 12.6 | 6.1 |
| $C_3H_8$ | 5.5 | 2.5 | 4.3 |
| $C_4H_8$ | 11.6 | 14.0 | 9.7 |
| n-$C_4H_{10}$ | 5.8 | 6.3 | 5.7 |
| i-$C_4H_{10}$ | 7.6 | 5.4 | 5.7 |
| $C_5$+ | 47.3 | 45.8 | 41.1 |
| Liquid Product Composition | | | |
| Aromatics | 53 | 37 | 42 |
| Olefins | 31 | 50 | 43 |
| Saturates | 16 | 13 | 15 |

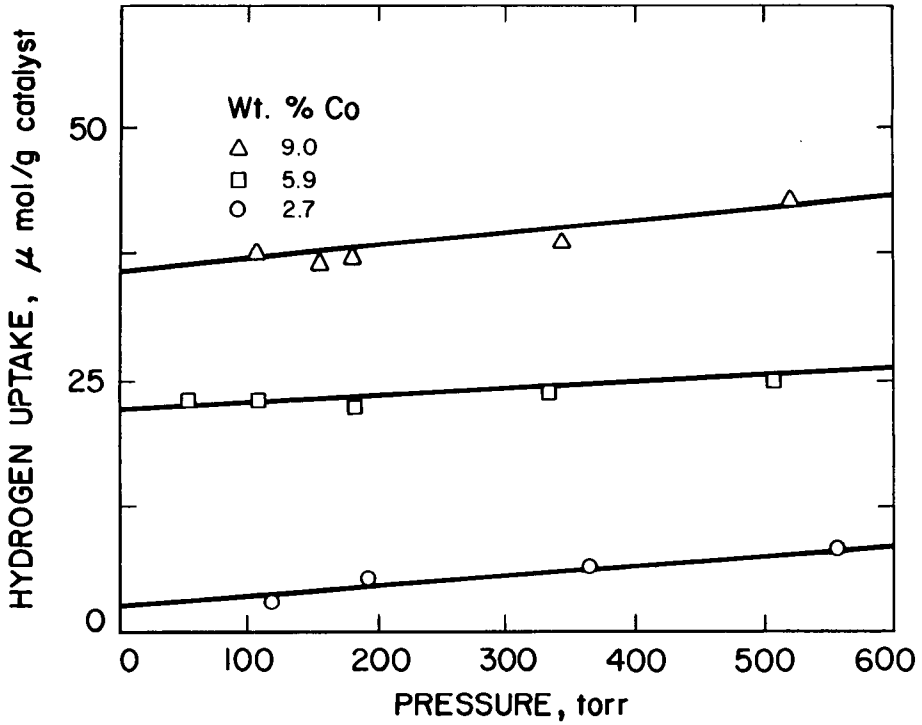


**Figure 1. Hydrogen adsorption isotherms at 100°C on Co/ZSM-5 catalysts.**

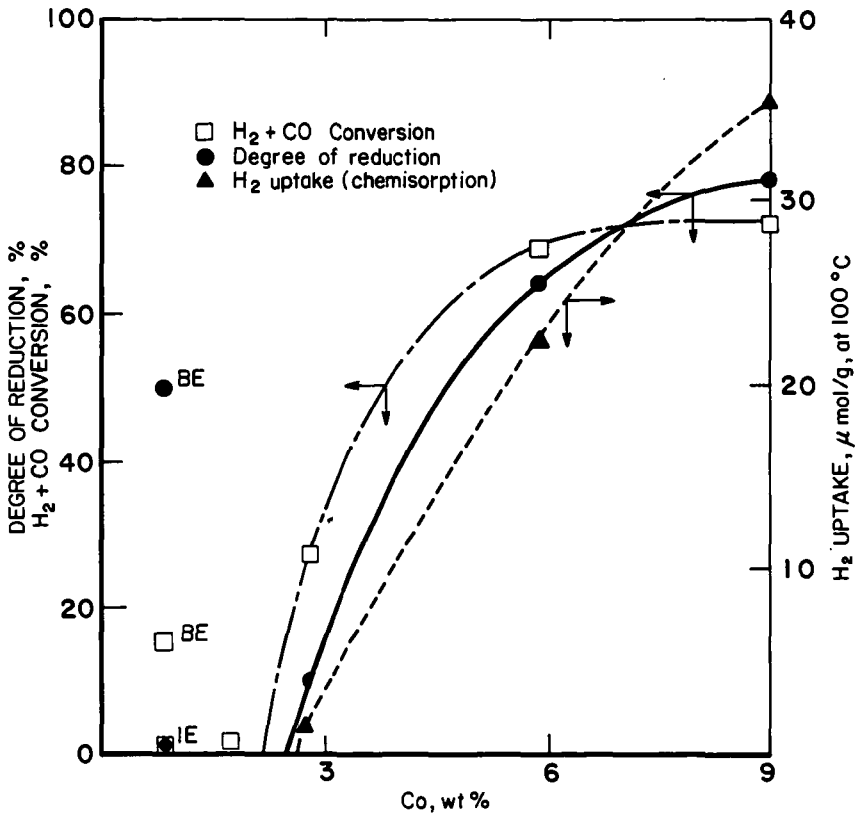


**Figure 2.** Degree of reduction, chemisorption and $H_2$ + CO conversion on Co/ZSM-5. IE: ion-exchanged, BE: back-exchanged.

BSI/3382

# A CURRENT VIEW OF THE MECHANISM FOR THE CATALYTIC GASIFICATION OF COAL CHAR

Bernard J. Wood and Kenneth M. Sancier

Materials Research Laboratory, SRI International
333 Ravenswood Avenue, Menlo Park, CA 94025

## INTRODUCTION

The addition of modest quantities of certain inorganic salts to coal substantially promotes its reactivity with steam or carbon dioxide. Because of the cost of the added salt and the addition of process steps for admixture and recovery, technoeconomic analysis predicts that this catalytic coal gasification process can be of practical value only in cases where the maximum process temperatures are limited by outside constraints.[1] One such case is the production of methane, where high equilibrium yield is favored by lower temperatures.[2] Current predictions, based on natural gas demand and reserves, suggest that methane from coal will not be needed in the next 25-50 years. Consequently, industrial interest in the catalytic gasification of coal, once high, has waned, and full-scale development of the process has been given lower priority.

Another potentially attractive application of the catalytic gasification process is the utilization conversion, storage, and transport of heat produced by a gas-cooled nuclear reactor where the attainable coolant temperature has an upper limit of about 950°C.[3] Implementation of this technology is being considered[4], but large-scale application lies some distance in the future.

However, the low probability of near term applications has not hampered scientific interest in the process. In the last few years, many investigators have studied the process, using a wide variety of approaches and tools. Since 1980 more than 100 papers have been published on the subject of the mechanism of catalytic gasification of char or carbon.[5] This investigative activity has given us sufficient insight into the process to suggest a detailed mechanism that defines the nature and role of the catalyst during gasification.

## CHARACTERISTICS OF CATALYST ACTION

Effective coal/char gasification catalysts are ionic salts with oxygen-bearing anions (or anions that are converted to oxygen-containing species under gasification conditions). The cations of the salt react

with the carbonaceous material to form a chemically and thermochemically distinct active species that mediates the gasification process. The anions of the salt may modify the pathway of formation of the active species, but for all effective salts this species is certainly formed at sub gasification temperatures.

There is broad agreement among recent investigators that the catalyst supplies oxygen to the carbon. Many investigators favor involvement of a redox cycle in which the catalyst is reduced by the carbon and oxidized by the gaseous reactant, but few speculate on a detailed mechanism. Nevertheless, there are a number of details of the gasification reaction system for which evidence is particularly strong:

- The working catalyst forms a liquid film that wets the carbon surface;
- The molten catalyst is a metal-rich (oxygen deficient) compound, probably an oxide, over which the metal vapor pressure has a characteristic equilibrium value;
- Chemical attack by the catalyst and during gasification occurs at the carbon atoms on edges of aromatic arrays;
- The reduction step occurs by donation by the carbon of an electron to the catalyst phase, neutralizing the cationic charge;
- A metal-oxygen-carbon complex analogous to a phenolate salt is a reaction intermediate;
- The intermediate is a precursor of gaseous CO production by a decarbonylation step that is likely rate governing.

## A PROPOSED MECHANISM

Based on these considerations, we have devised a detailed mechanism of catalyst action. Dispersion of the catalyst is a critical initial step that occurs at subgasification temperatures when the catalyst becomes a liquid film that wets the carbon and spreads over its exposed surface. Evidence for such a process comes from microscopic studies[6-8], measurements of surface area changes,[9,10] and the observed increase in electrical conductance upon heating of carbon-catalyst admixtures,[10] indicative of the formation of a phase with high charge carrier mobility. More quantitative information about the nature of alkali metal carbonates admixed with carbon is obtained from Knudsen cell mass spectrometry.[11] At about 900 K, both carbon-$K_2CO_3$ and carbon-$Cs_2CO_3$ admixtures in a Knudsen cell gradually lose oxygen, as evidenced by a progressive dimunition in the equilibrium partial pressures of CO and $CO_2$. At the same time the pressure of the alkali metal increases, indicating an increase in thermodynamic activity possibly produced by a change in metal/oxygen stoichiometry. Opposite changes occur when steam

or $CO_2$ is admitted to the Knudsen cell. These observations suggest that the liquid film in contact with the carbon is a non-stoichiometric oxide that contains an excess of the metal as atoms in a dissolved state. During gasification, the composition of the film is determined by a dynamic balance between a reducing process at the carbon-catalyst interface and an oxidizing process at the surface in contact with the gaseous reactant. The composition and characteristics of some Cs-rich oxides have been characterized as crystalline solids at room temperature.[12] At high temperatures they melt into liquid phases (for which free energies of formation have been evaluated) comprised of a higher oxide containing excess Cs.[13] Using the equilibrium partial pressures of Cs and CO measured over a $Cs_2CO_3$-carbon sample in the Knudsen cell, together with the published thermochemical data[13], we estimated the composition of the liquid phase to be $Cs_4O$.[11] A similar analysis of the $K_2CO_3$-carbon system was not possible because of the lack of thermochemical data at low oxygen partial pressures. By analogy, however, all alkali-metal-oxygen systems would be expected to behave in a parallel fashion. Further, very recent evidence of the conversion of $K_2CO_3$ to a nonstoichiometric oxide in the presence of carbon is provided by studies with isotope-labelled catalysts.[14]

The existence of an oxide with an excess of the alkali-metal component requires an equivalent number of oxygen vacancies. Thus, the affinity of this phase for reaction with an oxidizing gas will be proportional to the alkali metal activity. Oxygen ions produced by this reaction between the catalyst phase and an oxidizing gas are transported to the carbon/catalyst interface by diffusion, a process that is fast at gasification temperatures. One principal product of steam gasification, $H_2$, would be formed at the catalyst/steam interface.

The reaction steps occurring at the carbon/catalyst interface require some explanation because the carbon structure is comprised to some degree of planar aromatic arrays, and aromatic hydrocarbons are known to be quite unreactive toward oxide and hydroxide ions. Transmission electron microscopy[7,8] has confirmed that the catalyst interacts with carbon atoms located at the edges of the planar arrays, but the mechanism of the attachment remains obscure. We suggest that the initial reaction step is a simple electron transfer from the aromatic material to the alkali metal ion of the catalyst. Recently reported[15] measurements made in an electrochemical cell with a molten $Na_2CO_3$ electrolyte provide strong evidence for such an electron transfer step. In this work, the addition of graphite to the electrolyte (in the absence of air) rapidly shifted the rest potential of the cell from -0.511 to -1.348 V, indicative of the formation of an easily oxidized species, such as sodium metal, due to reduction of the sodium ions in the carbonate by the solid carbon. This process produces directly an excess of metal atoms in the catalyst and leaves the carbon array with a net positive charge, termed a radical cation. Such a species would be highly reactive toward the negatively charged oxygen ions in the catalyst. It is highly probably that reaction of the radical cation and the $O^=$ leads to formation of a phenolate ion, the presence of which in

the carbon array has been confirmed.[16] Indeed, phenolate ion structures would be stabilized by alkali metal ions in the molten catalyst film. The existence of some type of K-O-C structure has been suggested also on the basis of infrared spectra of partially gasified $K_2CO_3$-char admixtures.[17,18]

The rate of formation of CO during char gasification has been correlated with the concentration of phenolate groups.[19] This observation, in conjunction with the observed stability and steady state population of these groups at gasification temperatures,[20] suggests that decomposition of the phenolate groups is the rate-governing step in the catalytic gasification process. Decomposition may occur through conversion of the phenol functionality to the ketone followed by thermolytic decarbonylation.[10] This part of the gasification reaction pathway remains speculative, although such decarbonylation reactions have been observed to occur at high temperatures.[21]

## CONCLUSION

Inorganic salts composed of alkali metal cations and oxygen-bearing anions are effective catalysts for the steam or $CO_2$ gasification of coal char. Under gasification conditions the catalyst is converted to a nonstoichiometric oxide that is hgihly dispersed over the char surface as a liquid film. This catalyst film mediates the transfer of oxygen from the oxidizing gas to the char surface by way of a redox cycle. At the catalyst/char interface, electron donation by the char reduces the cation to a neutral metal atom dissolved in the catalyst, leaving a positively-charged radical cation on the char surface. The radical cation reacts readily with oxygen ions from the catalyst forming a phenolate functionality that is stabilized by the metal ions in the catalyst phase. The oxygen ions lost from the catalyst are replenished at the gas/catalyst interface by oxidation of the dissolved metal atoms by the oxidizing gas. The reactive intermediates are transported between gaseous oxidant and char by diffusion through the catalyst phase. CO is formed by decarbonylation of the phenolate species, a process that governs the rate of the gasification reaction.

## ACKNOWLEDGEMENT

Our studies of the mechanism of catalytic gasification of char were supported by the U.S. Department of Energy, Morgantown Energy Technology Center under Contract No. DE-AC21-80MC14593.

## REFERENCES

[1] H. Juntgen, Fuel, 62 (2), 234 (1983).

[2] N. C. Nahas, Fuel, 62 (2), 239 (1983).

[3] H. Kubiak, H. J. Schroter, A. Sulimma, and K. H. van Heek, Fuel, 62 (2), 242(1983).

[4] D. A. O'Sullivan, Chem. & Eng. News 62(10), 20-21 (1984).

[5] B. J. Wood and K. M. Sancier, Catal. Rev. Sci. Eng., in press (1984).

[6] H. Marsh and I. Mochida, Fuel, 60 (3), 231 (1981).

[7] D. J. Coates, J. W. Evans, A. L. Cabrera, G. A., Somorjai, and H. Heinemann, J. Catalysis, 80, 215 (1983).

[8] C. A. Mims, R. T. K. Baker, J. J. Chludzinski, and J. K. Pabst, Preprints Am. Chem. Soc. Fuel Chem. Div., 28 (1), 71 (1983).

[9] K. Otto, L. Bartosiewicz, and M. Shelef, Fuel, 58 (8), 565 (1979).

[10] B. J. Wood, R. H. Fleming, and H. Wise, Fuel, in press (1984).

[11] B. J. Wood, R. D. Brittain and K. H. Lau, Carbon, in press, (1984).

[12] A. Simon, Structure and Bonding (Berlin), 36, 81 (1979).

[13] C. F. Knights and B. A. Phillips, J. Nuclear Mat., 84, 196 (1979).

[14] J. M. Saber, J. L. Falconer, and L. F. Brown, private communication

[15] G. B. Dunks, Proceedings International Conference on Coal Science, Pittsburgh (1983), p. 457.

[16] C. A. Mims, K. D. Rose, M. T. Melchior, and J. K. Pabst, J. Am. Chem. Soc. 104, 6886 (1982).

[17] I. L. C. Freriks, H. M. H. van Wechem, J. C. M. Stuiver, and R. Bouwman, Fuel 60, 463 (1981).

[18] S. J. Yuh and E. E. Wolf, Fuel 62, 252 (1983).

[19] C. A. Mims and J. K. Pabst, Am. Chem. Soc. Fuel Chem. Div. Preprints 25(3), 258 (1980).

[20] C. A. Mims and J. K. Pabst, Fuel, 62 (2), 176 (1983).

[21] G. Schaden, Proc. 3rd. International Symp. Analyt. Pyrolisis, C.E.R. Jones and C. A. Cramers, editors, Elsevier, New York, 1977, p. 289.

# CARBONACEOUS AEROSOL FROM RESIDENTIAL WOOD COMBUSTION

J.A. Rau and J.J. Huntzicker

Department of Chemical, Biological, and Environmental Sciences
Oregon Graduate Center, 19600 N.W. Walker Road, Beaverton, Oregon 97006

Because of rising conventional energy prices wood has made a resurgence as a residential heating fuel. As a result residential wood smoke aerosols are becoming a major component of fine ambient aerosols in many areas. However, the quantification of the impact of residential wood smoke on the ambient aerosol concentration has been difficult because these aerosols are variable in composition and size and have no unique elemental tracers.

The purpose of this study has been to examine the size distribution and composition of residential wood smoke aerosols which have been sampled from cooled, diluted smoke plumes. Particles sampled in this manner should be more representative of wood smoke aerosols as they exist in the atmosphere than those sampled with EPA Method 5. Sampling was usually done about 1.5 m from the stack on days when the breeze was sufficient to move the plume in a mostly horizontal direction. Carbon dioxide measurements in the flue gas and in the sampled air indicated that the dilution factor was from 50 to 100. Air sampled from the plume was taken into a mixing chamber which was a 2 m long, 20 cm diameter aluminum pipe. Six samplers were located in the far end of the pipe. Each sampler consisted of a section of 5 cm diameter pipe which contained an impactor at its upstream end and a filter holder at its downstream end. Bypass air flow was maintained in the pipe to provide isokinetic sampling conditions. Single stage impactors with cut points at 2.5, 1.2, 0.6, 0.3, and 0.1 μm were used. One sampler which contained no impactor was used to sample the total aerosol concentration. Samples were collected on 37 mm diameter quartz filters for organic and elemental carbon analysis by thermo-optical carbon analysis (1,2). Samples were also collected on Teflon filters for analysis by x-ray fluorescence.

The composition and size distribution of wood smoke aerosols are a function of the burning conditions, fuel type, and stove type. In order to examine the range of variation of wood smoke characteristics, a series of tests which bracketed the typical burn conditions in residential applications was used. These consisted of burning hot (with the damper full open) and burning cool (with the damper closed). Testing was done with a conventional box type air-tight stove installed in a residence. The flue pipe was 20 cm in diameter and rose vertically from the top of the stove for a distance of 3.5 m. Enough air leaked into the stove with the damper closed to maintain combustion. This is a typical burn condition for residential heating. Fuel loads were usually three to four pieces of well-aged Douglas fir (quarter sections out of a 25 cm diameter log) that were about 0.5 m long. With this size fuel load (about one-quarter of the stove capacity) a reasonably intense fire could be maintained when the damper was fully open. By opening or closing the damper, operating conditions could be changed from hot operation to cool operation or vice versa. A test was started by adding the fuel load to a bed of coals. Sampling was started 10-15 minutes after fuel addition so as to be representative of average continuous burning where wood is added periodically to maintain a constant heat output. The length of the sampling period was chosen to obtain appropriate samples for analysis, usually 10-20 minutes.

In all cases the particles emitted during hot burning were significantly different from those emitted during cool burning. Qualitatively the mass loading in the sampled air was from three to six times greater for cool burn plumes than it was for hot burn plumes. However, the heat output of the stove was much less during a cool burn than it was for a hot burn. During hot burning the plume was almost invisible. The color of the collected aerosol was black and up to 60% of its carbon content was in the form of elemental carbon. The aerosol mass was primarily in

particles below 0.6 μm in diameter. Table 1 lists several aerosol mass distributions during hot burn conditions.

For cool burn tests the plume was always very visible and similar to plumes typically associated with residential wood burning. The color of the collected aerosol ranged from light yellow to dark tan. Table 2 shows some typical aerosol mass distributions as a function of size for cool burn tests.

In both hot and cool burns 70 ± 10% of the aerosol mass was carbon. In hot burns, as noted previously, elemental carbon predominated, but in cool burn conditions most of the carbon was organic. Size distributions of organic, elemental, and total (i.e., organic plus elemental carbon) are given in Table 3 for both hot and cool burn conditions. These results indicate that the mass distribution of carbon in cool burns is shifted to larger particle sizes relative to the hot burn cases.

In summary these results show that residential wood stove smoke particles are broadly distributed in the fine aerosol mode and that their composition can vary widely as a function of burn temperature. Studies on both source and ambient aerosols are continuing.

Acknowledgment. This research was sponsored in part by U.S. Environmental Protection Agency Grant R810091. The paper has not been subjected to EPA's peer review and therefore does not necessarily reflect the views of EPA.

References.

1. J.J. Huntzicker, R.L. Johnson, J.J. Shah, and R.A. Cary. "Analysis of Organic and Elemental Carbon in Ambient Aerosols by a Thermo-Optical Method." In Particulate Carbon Atmospheric Life Cycle, G.T. Wolff and R.L. Klimisch (editors), Plenum Press, New York, 1982, pp. 79-88.
2. R.L. Johnson, J.J. Shah, R.A. Cary, and J.J. Huntzicker. "An Automated Thermo-Optical Method for the Analysis of Carbonaceous Aerosol." In Atmospheric Aerosol: Source/Air Quality Relationships, E.S. Macias and P.K. Hopke (editors), American Chemical Society Symposium Series No. 167, American Chemical Society, Washington, D.C., 1981, pp. 223-233.

TABLE 1

Percent of aerosol mass in given size ranges for hot stove burns.

| Stove Temperature (°C) | <0.3 μm | 0.3-0.6 | 0.6-1.2 | >1.2 |
|---|---|---|---|---|
| 650 | 39 | 41 | 20 | 0 |
| 550 | 56 | 30 | 9 | 5 |
| 550 | 40 | 18 | 21 | 21 |
| 430 | 56 | 28 | 0 | 15 |

TABLE 2

Percent of aerosol mass in given size ranges for cool stove burns.

| Stove Temperature (°C) | <0.3 μm | 0.3-0.6 | 0.6-1.2 | >1.2 |
|---|---|---|---|---|
| 260 | 53 | 5 | 36 | 7 |
| 230 | 46 | 7 | 15 | 32 |
| 220 | 35 | 0 | 60 | 5 |
| 200 | 36 | 2 | 32 | 30 |

TABLE 3

Percent of organic, elemental, and total carbon in given aerosol size ranges.

| Size Range | Organic Carbon | Elemental Carbon | Total Carbon |
|---|---|---|---|
| | HOT BURN | | |
| <0.3 μm | 37 | 43 | 39 |
| 0.3-1.2 | 39 | 49 | 42 |
| >1.2 | 24 | 8 | 19 |
| | COOL BURN | | |
| <0.3 μm | 18 | 22 | 19 |
| 0.3-1.2 | 49 | 37 | 47 |
| >1.2 | 33 | 41 | 34 |